Atmos. Chem. Phys. Discuss., 13, 10961–11021, 2013
www.atmos-chem-phys-discuss.net/13/10961/2013/
doi:10.5194/acpd-13-10961-2013

Atmospheric Chemistry and Physics Discussions
Open Access

Impact of transport model errors on the global and regional methane emissions estimated by inverse modelling

R. Locatelli[1], P. Bousquet[1], F. Chevallier[1], A. Fortems-Cheney[1], S. Szopa[1], M. Saunois[1], A. Agusti-Panareda[2], D. Bergmann[3], H. Bian[4], P. Cameron-Smith[3], M. P. Chipperfield[5], E. Gloor[5], S. Houweling[6,7], S. R. Kawa[4], M. Krol[6,7,8], P. K. Patra[9], R. G. Prinn[10], M. Rigby[11,10], R. Saito[9], and C. Wilson[5]

[1]Laboratoire des Sciences du Climat et de l'Environnement (LSCE), UMR8212, Gif sur Yvette, France
[2]European Centre for Medium-Range Weather Forecasts, Shinfield Park, Reading, Berkshire RG2 9AX, UK
[3]Atmospheric, Earth, and Energy Division, Lawrence Livermore National Laboratory, 7000 East Avenue, Livermore, CA 94550, USA
[4]Goddard Earth Sciences and Technology Center, NASA Goddard Space Flight Center, Code 613.3, Greenbelt, MD 20771, USA
[5]Institute for Climate and Atmospheric Science, School of Earth and Environment, University of Leeds, Leeds, LS2 9JT, UK
[6]SRON Netherlands Institute for Space Research, Sorbonnelaan 2, 3584 CA Utrecht, the Netherlands

[7]Institute for Marine and Atmospheric Research Utrecht (IMAU), Princetonplein 5, 3584 CC Utrecht, the Netherlands
[8]Wageningen University and Research Centre, Droevendaalsesteeg 4, 6708 PB Wageningen, the Netherlands
[9]Research Institute for Global Change/JAMSTEC, 3173–25 Show-machi, Yokohama, 2360001, Japan
[10]Center for Global Change Science, Building 54, Massachusetts Institute of Technology, Cambridge, MA, 02139, USA
[11]School of Chemistry, University of Bristol, Bristol, BS8 1TS, UK

Received: 25 March 2013 – Accepted: 5 April 2013 – Published: 24 April 2013

Correspondence to: R. Locatelli (robin.locatelli@lsce.ipsl.fr)

Published by Copernicus Publications on behalf of the European Geosciences Union.

Abstract

A modelling experiment has been conceived to assess the impact of transport model errors on the methane emissions estimated by an atmospheric inversion system. Synthetic methane observations, given by 10 different model outputs from the international TransCom-CH_4 model exercise, are combined with a prior scenario of methane emissions and sinks, and integrated into the PYVAR-LMDZ-SACS inverse system to produce 10 different methane emission estimates at the global scale for the year 2005. The same set-up has been used to produce the synthetic observations and to compute flux estimates by inverse modelling, which means that only differences in the modelling of atmospheric transport may cause differences in the estimated fluxes.

In our framework, we show that transport model errors lead to a discrepancy of 27 Tg CH_4 per year at the global scale, representing 5 % of the total methane emissions. At continental and yearly scales, transport model errors have bigger impacts depending on the region, ranging from 36 Tg CH_4 in north America to 7 Tg CH_4 in Boreal Eurasian (from 23 % to 48 %). At the model gridbox scale, the spread of inverse estimates can even reach 150 % of the prior flux. Thus, transport model errors contribute to significant uncertainties on the methane estimates by inverse modelling, especially when small spatial scales are invoked. Sensitivity tests have been carried out to estimate the impact of the measurement network and the advantage of higher resolution models. The analysis of methane estimated fluxes in these different configurations questions the consistency of transport model errors in current inverse systems.

For future methane inversions, an improvement in the modelling of the atmospheric transport would make the estimations more accurate. Likewise, errors of the observation covariance matrix should be more consistently prescribed in future inversions in order to limit the impact of transport model errors on estimated methane fluxes.

Discussion Paper | Discussion Paper | Discussion Paper | Discussion Paper |

ACPD

13, 10961–11021, 2013

1 Introduction

Methane (CH_4) is the second most potent anthropogenic greenhouse gas in the atmosphere. While CH_4 mixing ratios varied between 350 and 800 parts per billion by volume (ppbv) over the past 650 000 yr (Spahni et al., 2005), current atmospheric methane levels have increased by more than 600 ppbv since 1950 (Etheridge et al., 1992) reaching, as a global mean, 1794 ppbv in 2009 (Dlugokencky et al., 2011). Methane is primarily emitted by biogenic sources linked to anaerobic decomposition of organic matter by methanogenic bacteria (wetlands, rice paddies, animal digestion, waste, landfills, termites). Emissions also involve thermogenic (fossil fuel extraction, transportation and use) and pyrogenic (biomass and biofuel burning) sources. Global emissions range from 500 Tg CH_4 yr^{-1} to 600 Tg CH_4 yr^{-1} (Denman et al., 2007). Typical ranges for estimates of global emissions for each process are of ±30 % (e.g. agriculture and waste) to more than ±100 % (fresh water emissions) (Kirschke et al., 2013). Atmospheric methane is removed mainly by the oxidation by OH radicals in the troposphere (90 % of the total sink). Additional sinks are the destruction in dry soils (methanotrophic bacteria), the oxidation in the stratosphere (OH, $O(^1D)$) and the oxidation by active chlorine in the marine planetary boundary layer (Allan et al., 2007). Knowing also that methane both plays a key role in air quality issues (Fiore et al., 2002) and is 23 times more effective as a greenhouse gas than CO_2 on a 100 yr horizon (Denman et al., 2007), it conduces to better understand and to quantify accurately the spatial and temporal patterns of methane sources and sinks. Besides, the disagreements between recent studies (Kai et al., 2011; Levin et al., 2012; Aydin et al., 2011; Simpson et al., 2012; Rigby et al., 2008; Montzka et al., 2011; Bousquet et al., 2006, 2011) explaining the weakening in the CH_4 growth rate from 2000 to 2006 and its increase since 2007 reinforces the idea that methane fluxes are poorly understood, both for the mean and their evolution in time.

Since the end of the nineties, several research groups have developed inverse methods to estimate CH_4 fluxes from global to regional scales by optimally combining CH_4

measurements with prior information and a chemistry transport model. Based on the Bayesian paradigm, a cost function is minimized either by analytical (Hein et al., 1997; Houweling et al., 1999; Bousquet et al., 2006; Chen and Prinn, 2006) or variational techniques (Pison et al., 2009; Meirink et al., 2008). The former solves the fluxes for large regions with a typical monthly time resolution and low-frequency surface observations as constraints. The latter uses a minimization technique which allows increasing the size of the inverse problem, assimilating high-frequency surface measurements and satellite data, and solving for fluxes at the model resolution, therefore avoiding most of the aggregation errors of large-region inversions (Kaminski et al., 2001). Although these two methods differ in the implementation, they are both based on chemistry transport models (CTM) to link emissions and sinks to atmospheric CH_4 concentrations and each CTM has its own characteristics: horizontal and vertical resolutions, boundary and initial conditions, meteorological drivers, advection scheme, subgrid parameterization schemes for convection, turbulence, or clouds, etc. Thus, it is legitimate to assess the sensitivity of estimated fluxes to the CTM used in the inversion process.

Since 1993, the TransCom experiment has compared transport models in their ability to represent trace gas concentrations in the atmosphere. Chronologically, TransCom community characterized the atmospheric transport for CO_2 (Law et al., 1996; Geels et al., 2007), SF_6 (Denning et al., 1999), ^{222}Rn (Taguchi et al., 2011), and more recently for CH_4 (Patra et al., 2011). Patra et al. (2011) focus on the reasons (misrepresentations of transport modelling, chemical loss, surface fluxes, etc.) of the unfaithful simulation of methane concentration in the atmosphere by CTMs. One major outcome of the TransCom experiment is that discrepancies in forcing meteorological fields and in model skills to reproduce atmospheric methane concentrations are important limitations to further improve our knowledge on sources and sinks of atmospheric trace gases. For the following, we define “forcing errors” as errors in the meteorological fields used by the CTMs and “model errors” as errors in the CTM itself. Thereafter, “transport model errors” will be used to group together forcing and model errors.

Currently, issues related to the modelling of atmospheric transport are all the more important that the skills of CTMs to simulate gas distribution properly are more and more sollicited in current inversions. Indeed, with the increasing spatial density of the surface observing networks and the apparition of satellite data, the limitation due to the lack of observations to constrain inverse systems should become less dominant, putting forcing and model errors in the forefront. For example, the availability of high-frequency observations in the continental planetary boundary layer (PBL) provide many more constraints to the inverse problems, but require that the atmospheric transport models simulate properly the transport within the PBL, which is a challenge for global models (Geels et al., 2007). More, the increasing availability of CH_4 retrievals provided by several satellites (SCIAMACHY, Frankenberg et al., 2008, GOSAT, Parker et al., 2011 and IASI, Crevoisier et al., 2012) requires a good representation of the vertical columns of trace gases (Houweling et al., 2010; Chevallier et al., 2010). Furthermore, as scientific objectives are moving towards estimating fluxes at smaller scales (regional to local), it will be required that we have more observations close to emissions sources. This implies that CTMs need to improve their ability to represent processes applying at these scales, or at least that forcing and model errors are properly quantified and accounted for in atmospheric inversions. If not, forcing and model errors would directly convert into biases in flux estimates. In this context, the main goal of our study is to quantify the impact of the misrepresentation of atmospheric processes by CTMs on the methane fluxes estimated by inverse modelling.

The importance to take in consideration forcing and model errors in current inversions has already been pointed out these last years. Gloor et al. (1999) even claimed that inversions were not reliable for CO_2 flux monitoring because of too large transport model errors. Engelen et al. (2002) showed that not accounting for these errors acts as a hard constraint on the inversion and produces incorrect solutions to the problem. At present, forcing and model errors are either approximately estimated or neglected in inversions, although studies aiming at quantifying these errors have showed a potentially high impact of these errors on the inverse estimates. For instance, Lin and

Discussion Paper | Discussion Paper | Discussion Paper | Discussion Paper |

ACPD
13, 10961–11021, 2013

Transport model errors in methane inversions

R. Locatelli et al.

Gerbig (2005) have assessed that horizontal wind were accountable for a 5 ppmv error in the modelling of CO_2 during summertime. Gerbig et al. (2008) focused on vertical mixing uncertainties for CO_2 inversions and highlighted large values of errors related to atmospheric transport. The impact of transport model errors on inversion has already been studied for CO_2 (Gurney et al., 2002; Baker et al., 2006), but, to our knowledge, no study has investigated this issue for CH_4 yet.

In this paper, we estimate the impact of transport model errors on inverted CH_4 fluxes using one variational inversion scheme, one flux scenario, and 10 different synthetic observation datasets built from the model database of the TransCom-CH_4 experiment (Patra et al., 2011). Section 2 describes the methodology and the synthetic data used for our inversions. Section 3.1 presents the main differences in the forward modelling of CH_4 concentrations due to the different CTMs used in Patra et al. (2011). Such differences are useful to better analyse the inversion results, exposed in Sect. 3.2. Sensitivity tests for the impact of CTM resolution (Sect. 3.3) and density of the measurement network (Sect. 3.4) on the inverse estimates are then proposed and analysed. Section 4 discusses the limitations of this synthetic experiment and the implication of our work to better represent transport model errors in future inversions.

2 Methodology

2.1 The synthetic experiment

This study follows the TransCom-CH_4 intercomparison experiment (Patra et al., 2011), which aimed to quantify the role of transport, flux distribution and chemical loss in simulating the seasonal cycle, synoptic variations and the diurnal cycle of CH_4 mixing ratio. For instance, large differences were found in the CH_4 mixing ratios simulated by the different CTMs in the transition region between the troposphere and the stratosphere, especially in the heights at which the vertical gradient is maximum. For each model participating to the TransCom-CH_4 experiment, a common protocol including the same emissions, the same sinks, and the same initial conditions was used. Therefore, simulated CH_4 mixing ratios for the different models should differ only because of the modelling of atmospheric transport by the CTMs (model errors) and the meteorology used to force them (forcing errors). The TransCom experiment does not allow separating these two effects as simulations testing different meteorological forcings were not provided. The database of the TransCom-CH_4 experiment includes outputs of hourly CH_4 mixing ratios at 166 surface stations, 6 tall towers, and 12 vertical profiles. We use daily averages of these model outputs as synthetic observations in a variational inversion system in order to quantify the impact of the different models on the inverted methane fluxes.

Figure 1 details the different steps of our method. First, ten forward simulations extracted from the TransCom-CH_4 database and forced by the monthly- and interannually varying emission dataset provided by Bousquet et al. (2006), are used to create synthetic daily-mean observation sets at selected sites (Patra et al., 2011). More details about the CTMs used to produce the forward simulations are provided in Sect. 2.2 and a full description of the selected sites is given in the Sect. 2.4. In a second step, the same emission scenario hereafter referred as “INV”, is combined with each synthetic observation dataset to feed the variational PYVAR inversion system, developed at LSCE (Chevallier et al., 2005). Knowing that PYVAR is based on LMDZ-SACS chemistry transport model (one of the models participating to the TransCom-CH_4 experiment), the synthetic observation dataset created using LMDZ-SACS simulations are considered as the “target” CH_4 mixing ratios and the INV scenario is considered as the “target” CH_4 emission patterns. We checked that using LMDZ-SACS synthetic observations in the inversion system gives exactly the target fluxes, within the numerical errors. Finally, in the last step of the experiment, CH_4 fluxes are estimated in all the grid cells of LMDZ-SACS for eight-day periods using the PYVAR inversion algorithm (see Sect. 2.3). By repeating the inversion process for each synthetic observation dataset, ten estimations of CH_4 fluxes are obtained. The comparison between these estimates provides a quantification of the influence of transport model errors on the CH_4 fluxes.

ACPD
13, 10961–11021, 2013

Indeed, the differences found in the inverted CH_4 fluxes are only due to discrepancies in the modelling of atmospheric transport by the different CTMs and in the meteorological analyses/reanalyses fields which drive them.

2.2 The chemistry transport models

Results from ten CTMs have been extracted from the TransCom-CH_4 experiment: ACTM (Patra et al., 2009), IFS (http://www.ecmwf.int/research/ifsdocs/CY37r2), IMPACT (Rotman, 2004), IMPACT-High resolution, LMDZ-SACS (version 4) (Hourdin et al., 2006; Pison et al., 2009), MOZART (version 4) (Emmons et al., 2010), PCTM (Kawa et al., 2004; Bian et al., 2006), TM 5 (Krol et al., 2005), TM 5-High resolution and TOMCAT (Chipperfield, 2006) (see Table 1 for more details).

These CTMs represent the diversity existing in the research community with horizontal resolutions ranging from $6^{\circ} \times 4^{\circ}$ (TM 5) to $0.7^{\circ} \times 0.7^{\circ}$ (IFS) and vertical discretisation ranging from 19 (LMDZ-SACS) to 67 layers (ACTM) with various coordinate systems (sigma vertical and hybrid-sigma pressure). Focusing on the representation of atmospheric transport, two groups of models can be distinguished: models using the meteorological fields from weather forecast analyses directly (IFS, IMPACT, MOZART, PCTM, TM 5 and TOMCAT) and models nudging towards horizontal winds and/or temperature (ACTM and LMDZ-SACS). The different CTMs also use a large diversity of meteorological drivers: different versions of NCEP/NCAR, NASA/GSFC/GEOS (version 4 and 5), ECMWF (ERA-40 and ERA-interim) and JCDAS.

Although the parameterization schemes implemented in the CTMs may have been slightly modified or adapted from the original scheme, the main schemes of the different CTMs are referenced in Table 2. The different schemes, implemented in the models of this experiment, describing advection are Lin and Rood (1996), Leer (1977), Hourdin and Armengaud (1999), Hortal (2002), Russell and Lerner (1981) and Prather (1986). Several CTMs use Holtslag (1993) or an adaptation of this scheme to parameterize the planetary boundary layer mixing. Walton et al. (1988), Laval et al. (1981), Louis (1979), Holtslag and Moeng (1991), Köhler et al. (2011) and Lock et al. (2000) are also used.

ACPD
13, 10961–11021, 2013

The parameterization of convection processes is implemented in the CTMs by using different adaptations of Tiedtke (1989), Zhang and McFarlane (1995), Bechtold et al. (2008), Rasch and Kristjánsson (1998) and Arakawa and Schubert (1974) schemes.

The CTMs used in this experiment are distinguished both by the reanalyses/analyses fields used to drive the CTMs and by their own characteristics (for example, resolution and parameterization schemes). As a result, this experiment studies the impact of these two contributions together (errors in meteorological drivers and errors in the models themselves) on the methane fluxes estimated by inverse modelling in Sect. 3.2.

Five additionnal model output datasets (ACCESS, Corbin, 2011, CAM, Gent et al., 2010, CCAM, Law et al., 2006, GEOS-Chem, Fraser et al., 2011; Pickett-Heaps et al., 2011 and NIES, Belikov et al., 2011, 2013) are available in the TransCom database. Unfortunately, some specific characteristics of these simulations make them unexploitable for our study. Indeed, all the contributions, but model and forcing errors, impacting the spread of the estimated fluxes have been left out from our work in order to only quantify the impact of transport model errors. For example, the different OH distribution used in GEOS-Chem simulation could bring additional difference in the chemical sink and lead to misinterpretation of the impact of transport model errors on the estimated fluxes. One can expect the same issue with CAM, CCAM and NIES since the total atmospheric burden of methane in these three models differs largely from the atmospheric burden of LMDZ-SACS. The differences of atmospheric burden between LMDZ-SACS and the discarded models ranges typically from 20 ppb up to 42 ppb. The atmospheric burden of LMDZ-SACS and of the other models retained in this study stay within 5 ppb, such differences being probably due to transport differences impacting the location and magnitude of the OH sink. ACCESS model which uses its own meteorology has also been removed, since it can not be expected to realistically simulate synoptic variations, which are essential in a inverse system using daily data (Sect. 2.4).

ACPD
13, 10961–11021, 2013

2.3 Set-up of the PYVAR-LMDZ-SACS inversion system

The PYVAR-LMDZ-SACS system (Chevallier et al., 2005; Pison et al., 2009) finds the optimal state of CH_4 fluxes given CH_4 observations and a background knowledge of fluxes using Bayesian inference formulated into a variational framework. The system iteratively minimizes the cost function J (Eq. 1) using an adjoint approach (Errico, 1997) and provides the best linear unbiased estimate, $\boldsymbol{x}$. The methane fluxes contained in $\boldsymbol{x}$ are optimized for eight-day periods in all the grid cells of the model. The cost function J is a measure of both the discrepancies between measurements and simulated mixing ratios and the discrepancies between the background fluxes and the fluxes to be estimated, weighted by their respective uncertainties, expressed in the covariance matrices **R** (measurement) and **B** (prior fluxes). The mathematical theory concepts are not detailed here, but may be found in Tarantola (2005).

$$J(\boldsymbol{x}) = (\boldsymbol{y} - \mathbf{H}\boldsymbol{x})^T \mathbf{R}^{-1} (\boldsymbol{y} - \mathbf{H}\boldsymbol{x}) + (\boldsymbol{x} - \boldsymbol{x}^b)^T \mathbf{B}^{-1} (\boldsymbol{x} - \boldsymbol{x}^b) \tag{1}$$

Hereafter, we describe the main characteristics of the system and we specify the inputs required to perform an inversion. **B** is the prior error covariance matrix with respect to the INV emission scenario. Its diagonal is filled in with the variances set to 100 % of the maximum over the eight neighboring cells during each month. Off diagonal terms of B (covariances) are based on correlation e-folding lengths (500 km over land and 1000 km over sea). No temporal correlations are considered here. $\boldsymbol{x}^b$ is the prior estimate using fluxes from the INV scenario.

H, the observation operator connecting the measurement space to the flux space, is represented here by the off-line version of the general circulation model of the Laboratoire de Meteorologie Dynamique (LMDZ) (Hourdin et al., 2006), complemented by a simplified chemistry module (SACS) to represent the oxidation chain of methane (Pison et al., 2009). Although the PYVAR-LMDZ-SACS system is able to constrain OH concentrations with methyl chloroform (CH_3CCl_3) measurements and to invert simultaneously OH fields and CH_4 fluxes, OH fields are prescribed from Spivakovsky et al.

(2000) (see the protocol of TransCom-CH_4 experiment described in Patra et al., 2010) in our experiment in order to focus only on transport model errors (modelling and forcing errors). Parameterized loss rates due to reactions of CH_4 with Cl and $O(^1D)$ have been taken from Patra et al. (2011). It is also noteworthy that LMDZ-SACS is run with a horizontal resolution of $2.5^\circ \times 3.75^\circ$ and with 19 vertical levels.

$\boldsymbol{y}$ contains the whole synthetic observations for the whole period of inversion. In theory, the **R** matrix accounts for all errors which contribute to the mismatches between measurements and simulated CH_4 mixing ratios at the stations. The **R** matrix may be splitted into two major parts (see Eq. 2): measurement and model errors. Measurement errors stand for instrumental errors, while model errors group representativity and transport model errors together.

$$\mathbf{R} = \mathbf{R}_{\text{measurement}} + \mathbf{R}_{\text{model}} \tag{2}$$

Instrumental errors quantify the errors between the mole fractions measured by an instrument and the target mole fractions. For instance, Bergamaschi et al. (2005) assume an instrumental uncertainty of 3 ppb for methane measured at surface stations.

Representation errors accounts for the misprepresentation of a single spatial and temporal measurement point by a gridbox of a 3-D model. Aggregation errors (Kaminski et al., 2001) are also included in representativity errors. Transport model errors group together the forcing errors and the model errors. Forcing errors represent the contribution of the errors included in the reanalyses/analyses fields which drive the chemistry transport models, while model errors quantify the misleading description of the physical processes (convection, diffusion, advection, ...) by the CTMs.

Here, **R** is considered as diagonal and variances are taken from Globalview-CH_4 (Globalview-CH_4, 2009). Errors in Globalview-CH_4 are computed at each site as the residual standard deviation (RSD) of the measurements about a smooth curve fitting them. We use the RSD at each site as a proxy of the transport model errors, assuming that the measurement sites with a lot of variability around the mean (e.g. continental sites) are more difficult to model especially for coarse global models (Geels

ACPD
13, 10961–11021, 2013

et al., 2007). This simple approach has been used previously in atmospheric inversions (Bousquet et al., 2006; Yver et al., 2011; Rodenbeck et al., 2003). Errors at stations where Globalview-CH_4 data were not available have been interpolated from stations presenting the same characteristics (background/polluted, Northern/Southern Hemisphere, coastal/continental). A detailed discussion on the specification of the **R** matrix takes place in Sect. 4. For now, it is important to keep in mind that both forcing and model errors are not taken explicitly in consideration in the **R** matrix of our experiment, which is usually the case in current inversions.

The period of analysis is the year 2005 but all the inversions are run with the same set-up over the extended period of July 2004–July 2006 to avoid edge effects. Indeed, we choose a 6 months period of spin-up to remove the influence of the initial conditions and the end of the inversion is stopped 6 months after the end of 2005 to have atmospheric constraints applying the fluxes at the end of 2005.

2.4 The synthetic observation data sets

The model outputs of the TransCom-CH_4 database are available at selected sites from the most widespread surface networks: Advanced Global Atmospheric Gases Experiment (AGAGE; http://agage.eas.gatech.edu), the NOAA Earth Research Laboratory, Global Monitoring Division (http://www.esrl.noaa.gov/gmd) and the Japan Meteorological Agency (http://www.jma.go.jp/jma/indexe.html). The synthetic observations are created at these following sites (Fig. 2a): 166 surface stations including 29 mobile stations (on ships), 6 vertical profiles (aircraft) and 12 tall towers. Some of these sites are continuous in-situ stations (red-filled circles). In some other locations, flasks are sampled on a weekly basis (empty red circles).

The blue triangles on Fig. 2a show the locations of tall towers and the green diamonds give the place of airplane measurements. For continuous stations, daily means have been computed to be assimilated in the PYVAR inversion framework. In order to mimic what is done in reality, 4 data per month are randomly chosen for each flask sampling site. As performed with real observations (Peylin et al., 2005), a specific treatment is done for flask sampling sites located at high altitudes (1500 m a.s.l.): the hour of the flask measurements is chosen in the early morning (7 a.m. LT), because, during the day, due to growing PBLs these sites could be polluted by local effects from the neighboring valleys, hardly simulated by global models. Towers are considered as continuous stations and are associated to daily-mean data. Two afternoon flights per week are considered for every airplane site, on a random basis. Besides, when several measurements are available in the same grid box, only the observation located at the highest altitude is kept in the inversion.

We performed reference inversions using an ideal future network (NET1), which contains 166 continuous surface stations. In this network, we assume that all flask sampling sites become continuous. Indeed, if the efforts and the fundings to develop and maintain surface networks are preserved (Houweling et al., 2012), more continuous stations should appear around the world in the next years bringing very valuable information for inversions (Law et al., 2002). No information on the CH_4 vertical distribution provided by tall towers or by airplanes are taken into consideration in the reference inversions.

However, inversions being highly sensitive to the measurements included in the PBL (Geels et al., 2007), two other networks have been tested. We consider a present-day surface network (NET2) with flask sampling sites (empty red circles) and continuous surface stations (filled red circles). The third network (NET3) adds airplane and tower data to NET2. This last network will give information on the contribution of PBL and tropospheric data on CH_4 flux estimates. The results are presented for NET1 in Sect. 3.2, and sensitivity tests using NET2 and NET3 are analysed in Sect. 3.4.

ACPD
13, 10961–11021, 2013

3 Results

3.1 Transport model discrepancies in forward modelling

We first analyse the differences between the simulated CH_4 mixing ratios for the TransCom models, considering LMDZ-SACS as a reference model because LMDZ-SACS is the CTM of the PYVAR inversion system. All CTMs have been forced by the same emission scenario (INV from Patra et al., 2011), the same OH fields and the same initial conditions, which imply that the spread in the CH_4 mixing ratio distribution given by the models is only due to differences in the meteorology and in the modelling of the atmospheric transport. Differences in reanalysis fields, horizontal and vertical resolutions, advection schemes and subgrid scale parameterizations (mixing in the boundary layer, convection scheme) are the possible causes of disagreement among CTMs. In this synthetic experiment, methane mixing ratios simulated by LMDZ-SACS are considered as the target and we analyse the spread of other models around LMDZ-SACS.

3.1.1 Synoptic variability

Figure 3 illustrates that continental stations, such as Karasevoe station (58.25° N; 82.40° E, Russia), show large differences in the magnitude of both the simulated seasonal cycles and the synoptic variability of CH_4 mixing ratio. Differences in the seasonal cycles may be related to differences in the covariance of surface emissions and transport in the PBLs through the rectifier effect mechanism (Denning et al., 1999) in relation with differences in the meteorological constraints and subgrid scale parameterizations of the models, although probably smaller for CH_4 than for CO_2. Phase differences observed in the synoptic variations can directly be related to the differences in the meteorology fields used by the models. Indeed the computation of correlations of CH_4 time series between CTMs shows that CTMs using similar meteorological drivers are more correlated with each others than with other models. For instance, methane time series simulated by IFS using ERA-interim reanalysis are highly correlated to TM 51 × 1 and

TM 5, which use ERA-interim reanalysis as well, with linear Pearson correlation coefficients of 0.92 and 0.84 respectively, whereas the average correlation of IFS with other models is only of 0.68.

First, we quantify the magnitude of the variability between the synthetic observations created with the TransCom models and the target CH_4 mixing-ratio generated by LMDZ-SACS for the first network considered (NET1, see Sect. 2.4) by computing the differences between the CH_4 mole fraction standard deviation (STD) of LMDZ-SACS and STD of other TransCom models at all surface stations. Discrepancies in the modelling of both the seasonal cycle amplitude and the synoptic variability contribute to the STD differences. We focus here only on the contribution of synoptic variability to the STD. We did so as it is expected to have higher impacts of transport modelling errors at continental stations, where synoptic variability dominates over seasonal changes. Indeed, the analysis of the STD at 16 continental stations shows that the values of STD related to synoptic variability (resp. related to seasonal cycle) are 87 % (resp. 42 %) of the total STD values.

Moreover, the relation between forward modelling analysis of synoptic variability and the expectations in the estimates by inverse modelling is straightforward: TransCom models simulating a larger synoptic variability (and consequently higher concentration peaks) than LMDZ-SACS at some stations are expected to give higher inverted fluxes within the area impacted by these stations. Hereafter, we call "synoptic STD", the STD related to synoptic variability when the seasonal cycle is removed from the time series. The map of the synoptic STD differences between LMDZ-SACS and the average of all the TransCom models ($\sigma_{\text{LMDZ-SACS}} - \overline{\sigma_{\text{TransCom}}}$; $\overline{\sigma_{\text{TransCom}}}$ being the average of all TransCom models "synoptic STD", $\sigma_{(\text{TransCom model})_i}$) is presented in Fig. 4. At first glance, a strong contrast is found between continental stations and stations with a dominant oceanic influence. Indeed, synoptic STD differences close to zero ppb (or slightly positive) are found at oceanic stations of the Southern Hemisphere. On the other hand, strong negative values of synoptic STD differences are found for continental stations of the Northern Hemisphere, suggesting that the amplitudes of

ACPD
13, 10961–11021, 2013

synoptic variability simulated by LMDZ-SACS are smaller than these simulated by the other TransCom models on average at these stations. Consequently, such discrepancies in the representation of synoptic variability by CTMs will have an impact on the fluxes estimated by inversion for the source regions that influence continental stations (north America, Europe, . . .). A previous study (Geels et al., 2007) has mentioned that LMDZ, as some other global models, underestimates synoptic variations of CO_2 concentrations and that the fast boundary layer ventilation of LMDZ could explain the small surface concentration peaks.

Moreover, a direct link appears between stations located in the vicinity of methane sources and stations deriving strong negative synoptic STD difference values. For instance, TVR (57.50° N; 33.75° E, Eastern Europe), LGB (52.8° N; 10.8° E, Europe), FRB (47.50° N; 7.50° E, Europe) and HIL (40.1° N; 87.9° W, East coast of the USA) are exposed to high sources of methane from the INV scenario (see Fig. 2b) and the mean of synoptic STD differences at these stations are respectively −20, −23, −35 and −15 ppb. Indeed, small scale transport processes, such as turbulence in the planetary boundary layer, which can hardly be fully represented by global CTMs have a large influence on the mole fractions simulated at stations close to large emission areas. On the contrary, stations far from any methane sources are mainly influenced by large scale transport of remote methane sources, which produces less differences between models. For example, the amplitude variability of TransCom models at AMS (37.9° S; 77.5° E, Indian Ocean) are equal on average to the amplitude simulated by LMDZ-SACS (synoptic STD difference is 0 ppb). At SUM (72.50° N; 37.50° E, Greenland), the synoptic STD difference is only of 2 ppb.

Stations may also be located either close to CH_4 sources or far from any CH_4 sources depending on the season. As an example, Fig. 3 presents the time series of daily CH_4 mixing ratio at Karasevoe (58.25° N; 82.40° E, Russia) for 2005. It shows a period with high concentrations from May to August, correlated to emissions from wetlands in this area at this period of the year, and a period of low concentrations during the boreal winter. The average for all the models of the STD during the high methane emission

ACPD
13, 10961–11021, 2013

period is 38 ppb, while the STD falls to 15 ppb only outside this period. Turbulent mixing in the boundary layer and convection are the main processes acting in this area during the summer period. The more methane is emitted, the more skills in the modelling of turbulent mixing and convection are sollicited. Consequently, as turbulent mixing and convection are differently represented by CTMs, models will be less in agreement during the period of high CH_4 emissions.

In order to better analyse the modelling of synoptic variability for each individual TransCom model, Fig. 5 presents the latitudinal distribution of synoptic STD differences at surface stations for each TransCom model. Each symbol represents the value of the synoptic STD difference ($\sigma_{\text{LMDZ-SACS}} - \sigma_{(\text{TransCom model})_i}$) at every surface station for a specific TransCom model. In the Southern Hemisphere, almost no distinction can be done between models: synoptic STD difference values are around 0 ppb. Consequently, all the models, except PCTM for few stations, simulate a variability with the same order of magnitude than LMDZ-SACS. In the Northern Hemisphere, MOZART, TM 51 × 1, IFS and PCTM exhibit the smallest synoptic STD difference values (negative values), meaning that these models simulate higher variability than LMDZ-SACS. On the contrary, TOMCAT is one of the model showing the smallest difference with LMDZ. These statements are especially true for continental stations of the Northern Hemisphere. As a consequence, it is expected to find, after inversion, higher emissions for MOZART, TM 51 × 1, IFS and PCTM and lower emissions for TOMCAT at least locally (around the stations) compared to the target INV emission scenario.

3.1.2 Inter-hemispheric (IH) exchange time

The inter-hemispheric (IH) exchange time is a good indicator to analyse large scale transport differences between transport models. Figure 6 presents the mean bias in simulated CH_4 mixing ratios at surface stations between LMDZ-SACS and other TransCom models ($y_{\text{LMDZ-SACS}} - \overline{y_{\text{TransCom}}}$). Negative biases are found at stations of the Northern Hemisphere meaning that CH_4 mixing ratios simulated by LMDZ-SACS are, on average, lower than those simulated by other TransCom models. On the contrary,

ACPD
13, 10961–11021, 2013

positive biases at surface stations of the Southern Hemisphere are found. Using SF_6 observations, LMDZ-SACS has been identified to have a fast IH exchange transport, characterised by an IH exchange time of 1.2 yr in the lower range of the ensemble of TransCom models (Patra et al., 2011) (see their Fig. 8). Therefore, LMDZ-SACS tends to transport more quickly (than other models) methane from the dominant emission zones of the Northern Hemisphere continents to the Southern Hemisphere. This fast IH transport produces the inferred negative biases in the north and positive biases in the south. One can expect that more emissions will be necessary over the northern continents, and/or less over the Southern continents when using LMDZ-SACS for inversions, the other models providing synthetic observations.

Figure 7 presents the latitudinal distribution of the bias between LMDZ-SACS and TransCom models ($y_{\text{LMDZ-SACS}} - y_{(\text{TransCom model})_i}$) at all surface stations for each TransCom model used in our study. In agreement with Fig. 6, most models exhibit a positive bias in the Southern Hemisphere. Moving towards stations of the Northern Hemisphere, biases decrease and become negative for several models due to the faster IH exchange time of LMDZ-SACS. More precisely, TM 5 (orange triangles) presents the larger gradients of biases between the stations of the Northern Hemisphere (difference of around −20 ppb in the Northern Hemisphere) and of the Southern Hemisphere (difference of around +10 ppb in the Southern Hemisphere). This is consistent with TM 5 having the longest IH exchange time in Patra et al. (2011). As a consequence, using synthetic observations from TM 5 in the inversions should increase the IH gradient of emissions, with less emissions in the Southern Hemisphere and more in the Northern Hemisphere.

3.2 Impact of transport model errors on inversions

Ten variational inversions have been performed, each being constrained by the synthetic observations generated with the model outputs extracted from the TransCom-CH_4 database (Patra et al., 2011). The same set-up (prior emissions from INV scenario, observation errors, prior errors, . . .) has been used for every inversion (see Sect. 2.3).

ACPD
13, 10961–11021, 2013

In order to keep the explanations clear in the following sections, each inversion is called by the name of the CTM used to generate the synthetic observations.

3.2.1 Global and hemispheric fluxes

Figure 8 presents the total estimated CH_4 fluxes for every model's inversion at global scale. The blue bars show the global CH_4 estimates for TransCom models and the red line points out the value of the target global CH_4 fluxes (523 Tg CH_4 yr^{-1}, INV scenario).

The CH_4 inverted fluxes for 2005 range from 523 Tg CH_4 yr^{-1} (MOZART inversion) to 550 Tg CH_4 yr^{-1} (PCTM inversion) with an average of 538 Tg CH_4 yr^{-1}. These results show that discrepancies in the modelling of atmospheric transport among the CTMs are responsible for a spread of 27 Tg CH_4 yr^{-1} (5 % of the target flux) on the inverted fluxes at the global scale. For comparison, the annual global methane emissions from rice paddies are estimated to be 37.5 Tg CH_4 in 2008 (EDGAR-v4.2, 2011). As for global methane emissions from biofuel and biomass burning, they have been estimated to 36 Tg yr^{-1} in the late nineties (Andreae and Merlet, 2001; van der Werf et al., 2010). Likewise, EDGAR-v4.2 (2011) infers methane emissions of 19.8 Tg from European countries of OECD in 2005. Consequently, in order to detect changes in methane emissions from a large region or to estimate the global emissions from some specific process, the impact of transport model errors on the inverse estimates is currently an important limitation.

It is noteworthy to mention that all inversions have derived higher or equal total fluxes at the global scale compared to the target flux. Indeed, as previously stated, the faster IH transport of LMDZ-SACS model compared to other models yields to higher average emissions in the Northern Hemisphere (+29 Tg CH_4 yr^{-1}) and to lower average emissions (−14 Tg CH_4 yr^{-1}) in the Southern Hemisphere. This leads to a global increase of 15 Tg CH_4 yr^{-1} in order to match the concentrations of the synthetic observations better. Table 3 exposes the estimates in the two hemispheres and the difference of emissions between the Northern and the Southern Hemisphere for each model. As

Discussion Paper | Discussion Paper | Discussion Paper | Discussion Paper |
ACPD
13, 10961–11021, 2013
Transport model errors in methane inversions
R. Locatelli et al.

expected, TM 5 derives the higher estimates in the Northern Hemisphere and the lower estimates in the Southern Hemisphere, which is consistent with the slower IH exchange time exhibited for TM 5 compared to LMDZ-SACS.

Time series of estimated CH_4 fluxes at the global scale (Fig. 9) shows general similar sesonal variations for all the CTMs with a peak of methane emissions during the boreal summer. The overlaid black line represents the target methane flux time series. Amplitudes of methane estimated fluxes variability reach 0.3 Tg CH_4 day^{-1}, which is about half of the amplitude of the seasonal cycle (0.7 Tg CH_4 day^{-1}). Moreover, it is noticeable that target fluxes are in the higher part of estimated emission range during boreal winter and in the lower part during boreal summer. Consequently, the magnitude of the seasonal cycle of CH_4 flux estimates is on average twice larger ($\sim$ 1.4 Tg CH_4 day^{-1}) than that of the target flux at the global scale. Indeed, the fast IH exchange time of LMDZ-SACS emphasises the derived seasonal cyle by increasing emissions in the Northern Hemisphere during boreal summer and decreasing emissions in the Southern Hemisphere during austral summer.

3.2.2 Regional fluxes

Figure 10 shows the estimations of CH_4 fluxes for seven continental regions (Europe, north America, Asia, south America, Africa, Oceania and Boreal Eurasian). Each symbol represents the estimation of one inversion using one synthetic observation dataset generated by one TransCom model. The numbers written next to the symbols give the spread of the estimation in percentage of the annual target flux and the black lines is the value of the target CH_4 fluxes for every region.

The spread of the inverted regional fluxes quantifies the impact of transport model errors on the estimation of methane fluxes inferred by atmospheric inversions at regional scales. Transport model errors produce much larger uncertainties on the methane emission estimates at the regional scale than at the global scale: from 23 % for Europe (16 Tg CH_4) to 48 % for south America (35 Tg CH_4). The spread in Africa is quite large (25 Tg CH_4) because estimates are splitted in two groups: inversions deriving

ACPD
13, 10961–11021, 2013

emissions around 95 Tg (ACTM, TOMCAT and TM 5) and those around 75 Tg (IFS, IMPACT, IMPACT 1 × 1, MOZART, PCTM and TM 51 × 1) for 2005.

Some characteristics of the TransCom models highlighted in Sect. 3.1 have a direct impact on the estimates at continental scale. First, the impact of the particularly fast IH exchange time of LMDZ-SACS compared to other TransCom models is also noticeable at continental scale. Indeed, for a vast majority of models, inversions derive higher estimates than the target fluxes in continental regions of the Northern Hemisphere (especially for north America). On the contrary, estimates of Southern Hemisphere continental regions tend to be lower than the target fluxes (especially for Oceania). This characteristic is particularly obvious for TM 5 which has been highlighted to simulate a particularly slow IH exchange time compared to the other models. Thus, the inversion using synthetic observations from TM 5 derives estimates for northern (southern) regions in the higher (lower) range of the estimates. This is the regional translation of the already noticed hemispheric changes.

Secondly, the spread in north America is quite large (37 %), which is largely amplified due to a large estimate of PCTM. It may be related to the characteristic of PCTM to simulate high concentration peaks at continental stations (see Sect. 3.1.1). On the contrary, TOMCAT simulating smaller synoptic variabilities than LMDZ-SACS, its estimates in Europe and in north America are in the lower range of the derived estimates. These results confirm that discrepancies in synoptic variability have an impact on the flux estimates in regions with many continental stations (Sect. 3.1.1).

Time series of weekly methane flux estimates are presented for one region of the Northern Hemisphere (Western Europe) and one region of the Southern Hemisphere (Oceania) (Fig. 11). The spread in estimated methane fluxes is much higher at regional scale than at the global scale (see Sect. 3.2.1) relatively to the amount of methane emitted in these regions. The flux variability in Western Europe has a magnitude twice higher ($\approx 0.1\,\mathrm{Tg\,CH_4\,day^{-1}}$) than the seasonal cycle of the target flux ($\approx 0.04\,\mathrm{Tg\,CH_4\,day^{-1}}$). Moreover, dispersion of flux estimates in Western Europe is slightly higher during winter months than during summer time. Indeed, extratropical

ACPD
13, 10961–11021, 2013

Transport model errors in methane inversions

R. Locatelli et al.

storm tracks, which influence directly atmospheric conditions in Western Europe, have stronger activities in winter than in summer: more uncertainties in wind fields provided by weather forecast centers are expected during this period. Difference in the modelling of shallow winter boundary layers can also contribute to this large variability among models.

The estimated flux variability amplitude in Oceania is less pronounced because the magnitude of methane emissions is much lower than in Western Europe. However, again, the impact of the IH transport is clearly seen in the inverted fluxes: the time series of the target flux in Oceania is in the upper range of the estimated CH_4 fluxes in agreement with the lower inverted emissions in the Southern Hemisphere regions, as expected (Sect. 3.1.2).

3.2.3 Spatial distribution of inverted fluxes

This section takes benefit of one major interest of inversions based on a variational approach: the ability to infer optimal fluxes at model's gridbox scale.

Figure 12 exposes the maps of the differences between the target CH_4 fluxes (INV scenario) and inverted CH_4 fluxes for each model at gridbox scale. A positive (negative) difference, from green to red colors (from yellow to blue), means that estimated fluxes by inversions using synthetic observations are larger (smaller, respectively) compared to the target CH_4 fluxes. First, inversions show regions with similar changes in the emissions compared to the target flux. For example, most inversions derive lower emissions than the INV scenario in south America, more or less around a north-south track. It is very clear for TOMCAT, PCTM and TM5. Some others models (IMPACT 1 × 1, IFS and TM5 1 × 1), characterized by a better horizontal resolution, show a dipole of emissions probably associated to the simulated position of the ITCZ (Intertropical Convergence Zone): they derive higher emissions than the target flux in the north of south America and lower fluxes in the south.

In other regions, all inversions derive mostly the same sign for emission changes but their geographical distribution within the region may be very different depending on the model. For example, inversions in north America derive higher emissions than the target methane flux for most models. However, higher emissions are derived on the east coast of the United States by IMPACT, IMPACT 1 × 1 and PCTM, on the west coast by IFS and TM 51 × 1 , and on both coast of the United States by MOZART and TM 5.

In Asia, Europe and Africa it is difficult to distinguish an identical pattern in the emissions estimated by all the inversions. For instance, in Africa, as it has been already noted in Sect. 3.2.2, two different behaviours characterize the analysed emissions: models suggesting an increase of emissions (ACTM, TM 5, TOMCAT) and models suggesting a decrease of emissions (all others). It is also important to notice that IFS and TM 51 × 1 have a similar spatial distribution of inverted fluxes probably related to the fact that they use the same meteorology fields and have a very close horizontal resolution.

To summarize the impact of transport model errors at gridbox scale, the Fig. 13 shows the map of the spread between all methane inverse estimates in percentage of the target flux. The regions previously identified with large discrepancies in the different methane estimates are highlighted here with grid cell differences up to 150 % of the target flux. For instance, we clearly see two patterns with large spreads in south America, reminding the dipole of emissions mentioned in the previous analysis. The west coast of the United States and the poorly constrained region of Eastern Siberia also show a large spread. We may also notice larger spreads in the gridbox surrounding some stations strongly constraining the inverse system. This is the case, for instance, at Cape Grim (40.68° S; 144.68° E, Australia, Oceania) and at Mount Kenya (0.06° S; 37.30° E, Kenya, Africa).

3.3 Sensitivity to the model horizontal resolution

The TM 5 and IMPACT simulations also included higher resolution versions (TM 51 × 1 and IMPACT 1 × 1) which allows investigating the impact of an increasing horizontal resolution on the derived methane fluxes.

First, STD due to synoptic variability for the high-resolution version of TM 5 and IMPACT are on average higher at continental stations of the Northern Hemisphere (see

Fig. 5). Indeed, we can assume that the increase of horizontal resolution improves the representation of locally high concentration gradients in the high methane emission regions. In order to quantify these STD differences between a high and a low resolution version of the CTMs for some stations exposed to high sources of methane, we average STD values for continental stations from the Northern Hemisphere. Fifteen stations close to high sources of methane have been selected. It is found that STD values related to synoptic variability are, on average, 15 ppb higher for TM 51 × 1 than for TM 5 and 9 ppb higher in the case of IMPACT 1 × 1 compared to IMPACT, what could have a direct impact on the global estimate by increasing the emissions of TM 51 × 1 and IMPACT 1 × 1 compared to TM 5 and IMPACT.

Concerning the inversion results, there is only 2 Tg yr^{-1} differences between estimates of TM 51 × 1 (547 Tg) and TM 5 (545 Tg) inversions and 3 Tg yr^{-1} between estimates of IMPACT 1 × 1 (537 Tg) and IMPACT (534 Tg) inversions at the global scale. The increase of the global CH_4 emission estimates between the high and the low resolution version of CTMs is in agreement with the previous analysis of STD values. However, we could expect to derive a difference between global estimates of TM 5 and TM 51 × 1 bigger than 2 Tg yr^{-1} since the STD gaps between these two versions may be large. Nevertheless, in Patra et al. (2011) (see their Fig. 8), it is shown that the IH exchange time of TM 51 × 1 (∼ 1.60 yr in 2005) is faster than for TM 5 (∼ 1.75 yr in 2005) which should result in a global estimate closer to the target global estimate. As a consequence, the impact of synoptic variability on the global estimate is balanced by the impact of IH exchange, which results in a slight increase of the global estimate of TM 51 × 1 compared to TM 5. The results are less clear for IMPACT/IMPACT 1 × 1 because the magnitude of these two effects (amplitude of synoptic variability and IH exchange) in the forward modelling study are less obvious than for TM 5 and TM 51 × 1.

The impact of horizontal resolution on the estimated methane fluxes may be relatively different at continental scale. Estimated fluxes in Europe and in north America are very close for TM 5/TM 51 × 1 (77 and 76 Tg CH_4 yr^{-1} in Europe; 101 and 99 Tg CH_4 yr^{-1} in north America) and IMPACT/IMPACT 1 × 1 (68 and 69 Tg CH_4 yr^{-1} in

Europe; 97 and 100 Tg CH_4 yr^{-1} in north America). The larger amplitude of the synoptic variability of TM 51 × 1 and IMPACT 1 × 1 does not convert in larger fluxes possibly because TM 5 and IMPACT are already much more variable than LMDZ-SACS over these continents. On the contrary, differences between estimates of TM 5/TM 51 × 1 and IMPACT/IMPACT 1 × 1 are relatively large in Africa (94 and 79 Tg CH_4 yr^{-1} for TM 5 versions and 81 and 72 Tg CH_4 yr^{-1} for IMPACT versions) and in Oceania (29 and 38 Tg CH_4 yr^{-1} for TM 5 versions and 35 and 40 Tg CH_4 yr^{-1} for IMPACT versions). Estimates in Asia and south America are characterized by large differences between TM 5 and TM 51 × 1 (131 and 125 Tg CH_4 yr^{-1} in Asia; 55 and 72 Tg CH_4 yr^{-1} in south America), and small differences between IMPACT and IMPACT 1 × 1 (113 and 109 Tg CH_4 yr^{-1} in Asia; 88 and 90 Tg CH_4 yr^{-1} in south America). These larger changes could be the trace of less constrained tropical regions.

3.4 Sensitivity to the measurement network

The fluxes inferred by atmospheric inversions are sensitive to the location and density of observations used to constrain them, especially with uneven networks. We have used two other networks (NET2 and NET3) to assess the sensitivity of the modelling and transport errors on estimated fluxes to the network. NET2 assumes a mix of flasks and continuous data similar to the current situation. NET3 adds tower and aircraft measurements on top of NET2.

Using NET2, the inverse system derives lower global estimates for all the synthetic datasets, except for IFS (Fig. 14). For instance, ACTM, IMPACT and TM 5 inverted methane fluxes drops to 523, 525 and 538 Tg in 2005 compared to respectively 533, 534 and 545 Tg in the case of NET1. More constraints should ideally bring the estimated fluxes closer to the target fluxes. In other words, one could expect NET1 results to be closer to the target than NET2 fluxes. This discrepancy will be discussed in Sect. 4.

ACPD
13, 10961–11021, 2013

Estimates in NET2 and NET3 configuration are very similar at the global scale, except for PCTM, IFS and the two high resolution versions of TM 5 and IMPACT. Generally, the number of tall towers and airplane measurements is too low compared to the number of surface stations to produce a significant difference between estimates from NET2 and NET3 at the global scale. However, the better horizontal resolution of IFS, IMPACT 1 × 1 and TM 51 × 1 may explain the differences obtained in the global estimates between NET2 and NET3 configuration. The differences seen for PCTM estimates may be explained by the very strong vertical gradient simulated by PCTM compared to the other models (Saito et al., 2013).

Moreover, in the NET3 configuration, the additional information provided by tall towers and airplane included in the inversions effectively reduce the spread in the regions where these additional data are available compared to the NET2 inversions (Fig. 15). The spread decreases from 27 Tg CH_4 to 16 Tg CH_4 and from 7 Tg CH_4 to 4 Tg CH_4 for respectively north America and Boreal Eurasian. In Europe, the spread does not change much between NET2 (20 Tg CH_4) and NET3 (21 Tg CH_4) although three tall towers and one airplane are available implying that inversions are already constrained enough by the high density of surface stations in this region. In regions where there are no additional synthetic observations in NET3 (south America, Africa and Oceania), inversions using NET3 synthetic observations are very similar to what obtained for NET2.

4 Discussion

The previous section shows that forcing and model errors have a significant impact on CH_4 fluxes estimated by inverse modelling at the global scale and even more at regional and gridbox scales. Besides, several results, highlighted in our study, question the way statistics errors are specified in atmospheric inversions, with possibly non-adapted errors in the **R** observation covariance matrix. For instance, a badly simulated IH exchange time can lead in biased interpretations of atmospheric signals in terms

ACPD
13, 10961–11021, 2013

of inverted fluxes if the errors do not fully account for this modelling imperfection. In Sect. 3.4, it is shown that NET1 estimates of the global CH_4 flux are further from the targeted flux as compared to NET2, even though more atmospheric constraints are considered in NET1 than in NET2 configuration. Adding more constraints, as done in NET1, better defines in time and space the regional gradients of concentrations between stations, which emphasize, in terms of cost to be reduced in J, the differences between LMDZ-SACS and the other models. Associated with a possibly wrong estimation of errors in the **R** matrix, especially concerning transport model errors, it can lead to an amplification of the impact of errors, leading to a larger increase of global emissions for NET1 compared to NET2. This effect is amplified by the fact that most stations moving from continuous to discontinuous (flask) when moving from NET1 to NET2 are remote stations with smaller model differences than continental continuous stations remaining in NET2. Moreover, it is also shown that discrepancies in synoptic variability at surface stations may result in different methane estimated fluxes in the area impacting these surface stations after transport. As highlighted in the Sect. 3.2.2, the PCTM estimate in north America is probably amplified by the fact that large discrepancies in the modelling of synoptic variability with LMDZ-SACS due to transport differences are not fully accounted for in the inversion. This ensemble of elements suggests a mis specification of statistic of errors in the **R** matrix.

Table 4 compares the errors at 25 stations, representative of the different types of stations encountered (background, polluted, coastal, continental, . . .), contained in the **R** matrix of Chen and Prinn (2006), Bergamaschi et al. (2005) and of our study based on Globalview-CH_4 (2009). The same order of magnitude for the errors is used in these studies, even if some large differences may be found at some specific stations. For instance, at Hegyatsal (Hungary) station, Chen and Prinn (2006) derive an error of 101.2 ppb while the error given by Bergamaschi et al. (2005) is of 26.5 ppb. The errors used in our study generally lay between errors given by inversions of Chen and Prinn (2006) and of Bergamaschi et al. (2005). This means that observation errors used in this study are overall comparable to those currently used in inversions. However, transport model errors in current inversions are generally not represented explicitely. Indeed, state-of-the-art inversions usually implement parameterizations of model errors, which quantify the misrepresentations of a surface station inside a larger grid box of the chemistry transport model. Chen and Prinn (2006) introduced a "mismatch" error term in inversion process, aiming to mimic the representation error. This term is computed at each measurement site as the standard deviation of the CH_4 mole fraction surrounding the observation site. Bergamaschi et al. (2005) took also in consideration a "mismatch" (or "representativity") term which is related to spatial and temporal gradients in all the directions. Some other studies approximate transport errors by the variance of observations, to take into account the fact that it is difficult for global transport models to represent properly large variations of the concentrations (Bousquet et al., 2006; Geels et al., 2007). Bergamaschi et al. (2005) also introduced a term accounting for potential deficiency of the model to simulate the diurnal cycle properly. These approaches, as the one used in our study, do not fully account for model and/or forcing errors confirming that observation errors in methane inversions may be misspecified.

Moreover, we only focus in this study on the diagonal terms of **R** matrix since as it has been explained in Sect. 2.3, observation variance/covariance matrix generally do not include cross-correlations when only uneven surface observations are used. Nevertheless, both temporal and spatial correlations could also improve the specifications of statistic errors and limit the impact of transport errors on the inverted estimates. For instance, we showed in Sect. 3.1 that spreads of fluxes temporal series in Western Europe may be higher in boreal winter due to intense activity of storms track, suggesting a spatial correlation of transport model errors in western Europe with errors over the Atlantic Ocean. One could also partially take in consideration the wrong representation of the IH transport by including spatial correlations between stations from the Southern Hemisphere (or/and from the Northern Hemisphere). Figure 3 also points out that transport model errors may vary significantly from one season to another depending on seasonal emissions, suggesting also to consider temporal correlation in measurement errors covariance matrix. However, properly taking correlations into account

ACPD
13, 10961–11021, 2013

slows dramatically down the inversion process. Chevallier (2007) proposed, for CO_2 inversions, to inflate variances in order to limit the impact of correlations on the accuracy of flux estimates. This method being computationally efficient may be an encouraging way to consider correlations in future methane inversions.

Finally, our study also faces additional limitations. First, one could question the development of an inverse modelling experiment assimilating synthetic observations in only one model but currently, it is difficult to lead an intercomparison of inverted fluxes with up-to-date methodologies (variational, ensemble methods, ...) with as many models as available in TransCom-CH_4 experiment, because it would require an inversion framework for each CTM with either an adjoint model (variational) or a large number of inversions (ensemble methods). It could also be discussed that using synthetic observations, the true transport model errors are not properly represented. Indeed, gaps between CH_4 mixing ratios simulated by different CTMs may be different from gaps between observed and simulated CH_4 mixing ratios (Stephens et al., 2007). Here, it is assumed that transport model errors are properly mapped by the large number of CTMs used in this experiment. Last but not least, the modelling of the different physical processes (advection, convection, turbulent mixing, ...) and characteristics of the models (resolutions, vertical coordinate systems, meteorological fields) contributing to transport model errors are considered all together and can hardly be quantitavely separated, although there are insights that IH transport difference play an important role here as LMDZ-SACS has one of the shortest IH exchange time. Additional knowledge given by different sensitivity tests and by the literature on the skills of each CTM to represent these different atmospheric processes would provide information to separate the specific contributions to transport model errors of forcing errors and model errors.

ACPD
13, 10961–11021, 2013

5 Conclusions

We present a modelling exercise, based on a variational inversion, to quantify the impact of transport model errors on methane emission estimates derived by inverse modelling.

Synthetic observations were created from 10 CTMs of the TransCom-CH_4 experiment, and used to constrain one atmospheric inversion framework with a common set-up. Therefore, inversion runs are only distinguished by the different simulated atmospheric transport generating the different synthetic observation data sets. The spread between the different inverted estimates shows that transport forcing and model errors have a significant impact on CH_4 fluxes estimates. It reaches 5 % of the total global CH_4 emissions for one year (27 Tg CH_4), ranges between 23 % and 48 % of emitted fluxes at regional scale and can reach 150 % at the model gridbox scale. Over the continents, patterns of emissions can be very different depending on the region and on the model used to generate synthetic observations. Consequently, our results show that transport model errors impact significantly the inverted methane budget at all scales, with an increasing impact when going from global to more local scales.

The need to improve chemical transport models in order to improve inverse methane estimates has also been greatly highlighted recently (Chevallier et al., 2010; Houweling et al., 2010; Saito et al., 2013). For instance, Saito et al. (2013) give some indications for the future development of more accurate CTMs by improving the modelling of inter-hemispheric transport in particular. Indeed, they show that the models with larger vertical gradients, coupled with slower horizontal transport, exhibit greater CH_4 inter-hemispheric gradients in the lower troposphere.

We also show that the misrepresentation of transport model errors in methane inversions can emphasize these modelling issues. Consequently, improved formulations for the observation covariance matrix **R**, taking more properly into account the transport model errors, in order to mitigate their impacts on the estimated methane fluxes have to be proposed in future work.

ACPD
13, 10961–11021, 2013

Acknowledgements. This work is supported by DGA (Direction Générale de l'Armement) and by CEA (Centre à l'Energie Atomique et aux Energies Alternatives). The research leading to the IFS results has received funding from the European Community's Seventh Framework Programme (FP7 THEME [SPA.2011.1.5-02]) under grant agreement n.283576 in the context of the MACC-II project (Monitoring Atmospheric Composition and Climate – Interim Implementation). The contribution by the LLNL authors was prepared under Contract DE-AC52-07NA27344, with different parts supported by the IMPACTS project funded by the US DOE (BER) and project (07-ERD-064) funded by the LDRD program at LLNL.

The publication of this article is financed by CNRS-INSU.

References

Allan, W., Struthers, H., and Lowe, D. C.: Methane carbon isotope effects caused by atomic chlorine in the marine boundary layer: global model results compared with Southern Hemisphere measurements, J. Geophys. Res., 112, D04306, doi:10.1029/2006JD007369, 2007. 10964

Andreae, M. O. and Merlet, P.: Emission of trace gases and aerosols from biomass burning, Global Biogeochem. Cy., 15, 955–966, doi:10.1029/2000GB001382, 2001. 10980

Arakawa, A. and Schubert, W.: Interaction of a cumulus cloud ensemble with the large-scale environment, Part I, J. Atmos. Sci., 31, 674–701, doi:10.1175/1520-0469(1974)031¡0674:IOACCE¿2.0.CO;2, 1974. 10970, 11004

Aydin, M., Verhulst, K. R., Saltzman, E. S., Battle, M. O., Montzka, S. A., Blake, D. R., Tang, Q., and Prather, M. J.: Recent decreases in fossil-fuel emissions of ethane and methane derived from firn air., Nature, 476, 198–201, doi:10.1038/nature10352, 2011. 10964

Baker, D. F., Law, R. M., Gurney, K. R., Rayner, P., Peylin, P., Denning, a. S., Bousquet, P., Bruhwiler, L., Chen, Y.-H., Ciais, P., Fung, I. Y., Heimann, M., John, J., Maki, T., Maksyutov, S., Masarie, K., Prather, M., Pak, B., Taguchi, S., and Zhu, Z.: TransCom 3 inversion intercomparison: Impact of transport model errors on the interannual variability of regional CO_2 fluxes, 1988–2003, Global Biogeochem. Cy., 20, GB1002, doi:10.1029/2004GB002439, 2006. 10967

Bechtold, P., Jung, T., Doblas-Reyes, F., Leutbecher, M., Rodwell, M. J., Vitart, F., and Balsamo, G.: Advances in simulating atmospheric variability with the ECMWF model: from synoptic to decadal time-scales, Q. J. Roy. Meteorol. Soc., 134, 1337–1351, doi:10.1002/qj.289, 2008. 10970, 11004

Belikov, D., Maksyutov, S., Miyasaka, T., Saeki, T., Zhuravlev, R., and Kiryushov, B.: Mass-conserving tracer transport modelling on a reduced latitude-longitude grid with NIES-TM, Geosci. Model Dev., 4, 207–222, doi:10.5194/gmd-4-207-2011, 2011. 10970

Belikov, D. A., Maksyutov, S., Krol, M., Fraser, A., Rigby, M., Bian, H., Agusti-Panareda, A., Bergmann, D., Bousquet, P., Cameron-Smith, P., Chipperfield, M. P., Fortems-Cheiney, A., Gloor, E., Haynes, K., Hess, P., Houweling, S., Kawa, S. R., Law, R. M., Loh, Z., Meng, L., Palmer, P. I., Patra, P. K., Prinn, R. G., Saito, R., and Wilson, C.: Off-line algorithm for calculation of vertical tracer transport in the troposphere due to deep convection, Atmos. Chem. Phys., 13, 1093–1114, doi:10.5194/acp-13-1093-2013, 2013. 10970

Bergamaschi, P., Krol, M., Dentener, F., Vermeulen, A., Meinhardt, F., Graul, R., Ramonet, M., Peters, W., and Dlugokencky, E. J.: Inverse modelling of national and European CH_4 emissions using the atmospheric zoom model TM 5, Atmos. Chem. Phys., 5, 2431–2460, doi:10.5194/acp-5-2431-2005, 2005. 10972, 10988, 10989, 11006

Bian, H., Kawa, S. R., Chin, M., Pawson, S., Zhu, Z., Rasch, P., and Wu, S.: A test of sensitivity to convective transport in a global atmospheric CO_2 simulation, Tellus B, 58, 463–475, doi:10.1111/j.1600-0889.2006.00212.x, 2006. 10969

Bousquet, P., Ciais, P., Miller, J. B., Dlugokencky, E. J., Hauglustaine, D. A., Prigent, C., Van der Werf, G. R., Peylin, P., Brunke, E.-G., Carouge, C., Langenfelds, R. L., Lathière, J., Papa, F., Ramonet, M., Schmidt, M., Steele, L. P., Tyler, S. C., and White, J.: Contribution of anthropogenic and natural sources to atmospheric methane variability., Nature, 443, 439–43, doi:10.1038/nature05132, 2006. 10964, 10965, 10968, 10973, 10989

Bousquet, P., Ringeval, B., Pison, I., Dlugokencky, E. J., Brunke, E.-G., Carouge, C., Chevallier, F., Fortems-Cheiney, A., Frankenberg, C., Hauglustaine, D. A., Krummel, P. B., Langenfelds, R. L., Ramonet, M., Schmidt, M., Steele, L. P., Szopa, S., Yver, C., Viovy, N., and Ciais, P.: Source attribution of the changes in atmospheric methane for 2006–2008, Atmos. Chem. Phys., 11, 3689–3700, doi:10.5194/acp-11-3689-2011, 2011. 10964

Chen, Y.-H. and Prinn, R. G.: Estimation of atmospheric methane emissions between 1996 and 2001 using a three-dimensional global chemical transport model, J. Geophys. Res., 111, 1–25, doi:10.1029/2005JD006058, 2006. 10965, 10988, 10989, 11006

Chevallier, F.: Impact of correlated observation errors on inverted CO_2 surface fluxes from OCO measurements, Geophys. Res. Lett., 34, L24804, doi:10.1029/2007GL030463, 2007. 10990

Chevallier, F., Fisher, M., Peylin, P., Serrar, S., Bousquet, P., Bréon, F.-M., Chédin, A., and Ciais, P.: Inferring CO_2 sources and sinks from satellite observations: Method and application to TOVS data, J. Geophys. Res., 110, 1–13, doi:10.1029/2005JD006390, 2005. 10968, 10971

Chevallier, F., Feng, L., Bösch, H., Palmer, P. I., and Rayner, P. J.: On the impact of transport model errors for the estimation of CO_2 surface fluxes from GOSAT observations, Geophys. Res. Lett., 37, L21803, doi:10.1029/2010GL044652, 2010. 10966, 10991

Chipperfield, M. P.: New version of the TOMCAT/SLIMCAT off-line chemical transport model: intercomparison of stratospheric tracer experiments, Q. J. Roy. Meteor. Soc., 132, 1179–1203, doi:10.1256/qj.05.51, 2006. 10969

Corbin, K. D. and Law, R. M.: Extending atmospheric CO_2 and tracer capabilities in ACCESS, CAWCR Technical Report No. 035, 2011. 10970

Crevoisier, C., Nobileau, D., Armante, R., Crépeau, L., Machida, T., Sawa, Y., Matsueda, H., Schuck, T., Thonat, T., Pernin, J., Scott, N. A., and Chédin, A.: The 2007–2011 evolution of tropical methane in the mid-troposphere as seen from space by MetOp-A/IASI, Atmos. Chem. Phys. Discuss., 12, 23731–23757, doi:10.5194/acpd-12-23731-2012, 2012. 10966

Denman, Marquis, M., Averyt, K. B., and Kingdom, U.: Couplings between changes in the climate system and biogeochemistry, the physical basis of climate change, in: Contribution of Working Group I to the Fourth Assessment Report of the IPCC, edited by: Solomon, S., Qin, D., Manning, M., Chen, Z., Marquis, M., Averyt, K. B., Tignor, M., and Miller, H. L., Cambridge University Press, Cambridge, UK and New York, NY, USA, 500–587, 2007. 10964

Denning, A. S., Holzer, M., Gurney, K. R., Heimann, M., Law, R. M., Rayner, P. J., Fung, I. Y., Fan, S.-M., Taguchi, S., Friedlingstein, P., Balkanski, Y., Taylor, J., Maiss, M., and Levin, I.: Three-dimensional transport and concentration of SF_6, a model intercomparison study

(TransCom 2), Tellus B, 51, 266–297, doi:10.1034/j.1600-0889.1999.00012.x, 1999. 10965, 10975

Desroziers, G., Berre, L., Chapnik, B., and Poli, P.: Diagnosis of observation, background and analysis-error statistics in observation space, Q. J. Roy. Meteor. Soc., 131, 3385–3396, doi:10.1256/qj.05.108, 2005.

Dlugokencky, E. J., Nisbet, E. G., Fisher, R., and Lowry, D.: Global atmospheric methane: budget, changes and dangers., Philos. T. R. Soc. A., 369, 2058–72, doi:10.1098/rsta.2010.0341, 2011. 10964

Emission Database for Global Atmospheric Research (EDGAR), JRC/PBL (Joint Research Center of the European Commission/Netherlands Environmental Assessment Agency), release version 4.2, available at: http://edgar.jrc.ec.europa.eu (last access: April 2013), 2011. 10980

Emmons, L. K., Walters, S., Hess, P. G., Lamarque, J.-F., Pfister, G. G., Fillmore, D., Granier, C., Guenther, A., Kinnison, D., Laepple, T., Orlando, J., Tie, X., Tyndall, G., Wiedinmyer, C., Baughcum, S. L., and Kloster, S.: Description and evaluation of the Model for Ozone and Related chemical Tracers, version 4 (MOZART-4), Geosci. Model Dev., 3, 43–67, doi:10.5194/gmd-3-43-2010, 2010. 10969

Engelen, R. J., Denning, A. S., and Gurney, K. R.: On error estimation in atmospheric CO_2 inversions, J. Geophys. Res., 107, 4635, doi:10.1029/2002JD002195, 2002. 10966

Errico, R.: What is an adjoint model?, B. Am. Meteorol. Soc., 78, 2577–2591, doi:10.1175/1520-0477(1997)078¡2577:WIAAM¿2.0.CO;2, 1997. 10971

Etheridge, D., Pearman, G., and Fraser, P.: Changes in tropospheric methane between 1841 and 1978 from a high accumulation rate Antarctic ice core, Tellus B, 44B, 282–294, doi:10.1034/j.1600-0889.1992.t01-3-00006.x, 1992. 10964

Fiore, A. M., Jacob, D. J., Field, B. D., Streets, D. G., Fernandes, S. D., and Jang, C.: Linking ozone pollution and climate change: the case for controlling methane, Geophys. Res. Lett., 29, 25-1–25-4, doi:10.1029/2002GL015601, 2002. 10964

Frankenberg, C., Bergamaschi, P., Butz, A., Houweling, S., Meirink, J. F., Notholt, J., Petersen, A. K., Schrijver, H., Warneke, T., and Aben, I.: Tropical methane emissions: a revised view from SCIAMACHY onboard ENVISAT, Geophys. Res. Lett., 35, L15811, doi:10.1029/2008GL034300, 2008. 10966

Fraser, A., Miller, C. C., Palmer, P. I., Deutscher, N. M., Jones, N. B., and Griffith, D. W. T.: The Australian methane budget: interpreting surface and train-borne measurements using a chemistry transport model, J. Geophys. Res., 116, D20306, doi:10.1029/2011JD015964, 2011. 10970

Geels, C., Gloor, M., Ciais, P., Bousquet, P., Peylin, P., Vermeulen, A. T., Dargaville, R., Aalto, T., Brandt, J., Christensen, J. H., Frohn, L. M., Haszpra, L., Karstens, U., Rödenbeck, C., Ramonet, M., Carboni, G., and Santaguida, R.: Comparing atmospheric transport models for future regional inversions over Europe – Part I: mapping the atmospheric CO_2 signals, Atmos. Chem. Phys., 7, 3461–3479, doi:10.5194/acp-7-3461-2007, 2007. 10965, 10966, 10972, 10974, 10977, 10989

Gent, P., Yeager, S., Neale, R., Levis, S., and Bailey, D.: Improvements in a half degree atmosphere/land version of the CCSM, Clim. Dynam., 34, 819–833, 1–30, doi:10.1007/s00382-009-0614-8, 2010. 10970

Gerbig, C., Körner, S., and Lin, J. C.: Vertical mixing in atmospheric tracer transport models: error characterization and propagation, Atmos. Chem. Phys., 8, 591–602, doi:10.5194/acp-8-591-2008, 2008. 10967

GLOBALVIEW-CH4: Cooperative Atmospheric Data Integration Project – Methane, CD-ROM, NOAA ESRL, Boulder, Colorado,available at: ftp://ftp.cmdl.noaa.gov, path: ccg/ch4/GLOBALVIEW (last access: April 2013), 2009. 10972, 10988

Gloor, M., Fan, S.-M., Pacala, S., Sarmiento, J., and Ramonet, M.: A model-based evaluation of inversions of atmospheric transport, using annual mean mixing ratios, as a tool to monitor fluxes of nonreactive trace substances like CO_2 on a continental scale, J. Geophys. Res., 104, 14245, doi:10.1029/1999JD900132, 1999. 10966

Gurney, K. R., Law, R. M., Denning, A. S., Rayner, P. J., Baker, D., Bousquet, P., Bruhwilerk, L., Chen, Y.-H., Ciais, P., Fan, S., and Fung, I. Y.: Towards robust regional estimates of CO_2 sources and sinks using atmospheric transport models, Nature, 415, 626–630, doi:10.1038/415626a, 2002. 10967

Hein, R., Crutzen, P. J., and Heimann, M.: An inverse modeling approach to investigate the global atmospheric methane cycle, Global Biogeochem. Cy., 11, 43–76, doi:10.1029/96GB03043, 1997. 10965

Holtslag, A.: Local versus nonlocal boundary-layer diffusion in a global climate model, J. Climate, 6, 1690–1698, doi:10.1175/1520-0442(1993)006<1825:LVNBLD>2.0.CO;2, 1993. 10969, 11004

ACPD
13, 10961–11021, 2013

Transport model errors in methane inversions

R. Locatelli et al.

Holtslag, A. and Moeng, C.-H.: Eddy diffusivity and countergradient transport in the convective atmospheric boundary layer, J. Atmos. Sci., 48, 1690–1698, doi:10.1175/1520-0469(1991)048<1690:EDACTI>2.0.CO;2, 1991. 10969, 11004

Hortal, M.: The development and testing of a new two-time-level semi-Lagrangian scheme (SETTLS) in the ECMWF forecast model, Q. J. Roy. Meteor. Soc., 2, 1671–1687, doi:10.1002/qj.200212858314, 2002. 10969, 11004

Hourdin, F. and Armengaud, A.: The use of finite-volume methods for atmospheric advection of trace species, Part I: test of various formulations in a general circulation model, Mon. Weather Rev., 127, 822–837, doi:10.1175/1520-0493(1999)127<0822:TUOFVM>2.0.CO;2, 1999. 10969, 11004

Hourdin, F., Musat, I., Bony, S., Braconnot, P., Codron, F., Dufresne, J.-L., Fairhead, L., Filiberti, M.-A., Friedlingstein, P., Grandpeix, J.-Y., Krinner, G., LeVan, P., Li, Z.-X., and Lott, F.: The LMDZ4 general circulation model: climate performance and sensitivity to parametrized physics with emphasis on tropical convection, Clim. Dynam., 27, 787–813, doi:10.1007/s00382-006-0158-0, 2006. 10969, 10971

Houweling, S., Kaminski, T., Dentener, F., Lelieveld, J., and Heimann, M.: Inverse modeling of methane sources and sinks using the adjoint of a global transport model, J. Geophys. Res., 104, 26137, doi:10.1029/1999JD900428, 1999. 10965

Houweling, S., Aben, I., Breon, F.-M., Chevallier, F., Deutscher, N., Engelen, R., Gerbig, C., Griffith, D., Hungershoefer, K., Macatangay, R., Marshall, J., Notholt, J., Peters, W., and Serrar, S.: The importance of transport model uncertainties for the estimation of CO_2 sources and sinks using satellite measurements, Atmos. Chem. Phys., 10, 9981–9992, doi:10.5194/acp-10-9981-2010, 2010. 10966, 10991

Houweling, S., Badawy, B., and Baker, D.: Iconic CO_2 time series at risk, Science, 337, 1038–1040, doi:10.1126/science.337.6098.1038-b, 2012. 10974

Kai, F. M., Tyler, S. C., Randerson, J. T., and Blake, D. R.: Reduced methane growth rate explained by decreased Northern Hemisphere microbial sources., Nature, 476, 194–197, doi:10.1038/nature10259, 2011. 10964

Kaminski, T., Rayner, P. J., Heimann, M., and Enting, I. G.: On aggregation errors in atmospheric transport inversions, J. Geophys. Res., 106, 4703, doi:10.1029/2000JD900581, 2001. 10965, 10972

ACPD
13, 10961–11021, 2013

Transport model errors in methane inversions

R. Locatelli et al.

Kawa, S. R., Erickson III, D. J., Pawson, S., and Zhu, Z.: Global CO_2 transport simulations using meteorological data from the NASA data assimilation system, J. Geophys. Res., 109, D18312, doi:10.1029/2004JD004554, 2004. 10969

Kirschke, S., Bousquet, P., Ciais, P., Saunois, M., Bergamaschi, P., Bergmann, D., Bruhwiler, L., Cameron-Smith, P., Canadell, J. G., Castaldi, S., Chevallier, F., Dlugokencky, E. J., Feng, L., Fraser, A., Heimann, M., Hodson, E. L., Houweling, S., Josse, B., Lamarque, J.-F., Le Quére, C., Naik, V., Palmer, P. I., Pison, I., Plummer, D., Poulter, B., Ringeval, B., Santini, M., Schmidt, M., Shindell, D. T., Spahni, R., Strode, S. A., Sudo, K., Szopa, S., van der Werf, G. R., Voulgarakis, A., wvan Weele, M., Williams, J. E., and Zeng, G.: Three decades of methane sources and sinks: budgets and variations, Nat. Geosci., submitted, 2013. 10964

Köhler, M., Ahlgrimm, M., and Beljaars, A.: Unified treatment of dry convective and stratocumulus-topped boundary layers in the ECMWF model, Q. J. Roy. Meteor. Soc., 137, 43–57, doi:10.1002/qj.713, 2011. 10969, 11004

Krol, M., Houweling, S., Bregman, B., van den Broek, M., Segers, A., van Velthoven, P., Peters, W., Dentener, F., and Bergamaschi, P.: The two-way nested global chemistry-transport zoom model TM 5: algorithm and applications, Atmos. Chem. Phys., 5, 417–432, doi:10.5194/acp-5-417-2005, 2005. 10969

Laval, K., R. Sadourny and Y. Serafini, Land surface processes in a simplified general circulation model, Geophys. Astro. Fluid, 17, 129–150, 1981. 10969, 11004

Law, R., Rayner, P., Denning, A. S., Erickson, D., Fung, I. Y., Heimann, M., Piper, S. C., Ramonet, M., Taguchi, S., Taylor, J. A., Trudinger, C. M., and Watterson, I. G.: Variations in modeled atmospheric transport of carbon dioxide and the consequences for CO_2 inversions, Global Biogeochem. Cy., 10, 783–796, doi:10.1029/96GB01892, 1996. 10965

Law, R. M., Rayner, P. J., Steele, L. P., and Enting, I. G.: Data and modelling requirements for CO_2 inversions using high-frequency data, Tellus B, 55, 512–521, doi:10.1034/j.1600-0889.2003.00029.x, 2002. 10974

Law, R. M., Kowalczyk, E. A., and Wang, Y.-P.: Using atmospheric CO_2 data to assess a simplified carbon-climate simulation for the 20th century, Tellus B, 58, 427–437, doi:10.1111/j.1600-0889.2006.00198.x, 2006. 10970

Leer, B. V.: Towards the ultimate conservative difference scheme. I V. A new approach to numerical convection, J. Comput. Phys., 23, 276–299, doi:10.1016/0021-9991(77)90095-X, 1977. 10969, 11004

Levin, I., Veidt, C., Vaughn, B. H., Brailsford, G., Bromley, T., Heinz, R., Lowe, D., Miller, J. B., Poß, C., and White, J. W. C.: No inter-hemispheric δ13CH_4 trend observed., Nature, 486, E3–4; discussion E4, doi:10.1038/nature11175, 2012. 10964

Lin, J. C. and Gerbig, C.: Accounting for the effect of transport errors on tracer inversions, Geophys. Res. Lett., 32, L01802, doi:10.1029/2004GL021127, 2005. 10966

Lin, S. and Rood, R.: Multidimensional flux-form semi-Lagrangian transport schemes, Mon. Weather Rev., 124, 2046–2070, doi:10.1175/1520-0493(1996)124<2046:MFFSLT>2.0.CO;2, 1996. 10969, 11004

Lock, A., Brown, A., and Bush, M.: A new boundary layer mixing scheme, Part I: scheme description and single-column model tests, Mon. Weather Rev., 128, 3187–3199, doi:10.1175/1520-0493(2000)128<3187:ANBLMS>2.0.CO;2, 2000. 10969, 11004

Louis, J.: A parametric model of vertical eddy fluxes in the atmosphere, Bound.-Lay. Meteorol., 7, 187–202, doi:10.1007/BF00117978, 1979. 10969, 11004

Meirink, J. F., Bergamaschi, P., and Krol, M. C.: Four-dimensional variational data assimilation for inverse modelling of atmospheric methane emissions: method and comparison with synthesis inversion, Atmos. Chem. Phys., 8, 6341–6353, doi:10.5194/acp-8-6341-2008, 2008. 10965

Montzka, S. A., Dlugokencky, E. J., and Butler, J. H.: Non-CO_2 greenhouse gases and climate change., Nature, 476, 43–50, doi:10.1038/nature10322, 2011. 10964

Parker, R., Boesch, H., Cogan, A., Fraser, A., Feng, L., Palmer, P. I., Messerschmidt, J., Deutscher, N., Griffith, D. W. T., Notholt, J., Wennberg, P. O., and Wunch, D.: Methane observations from the Greenhouse Gases Observing SATellite: Comparison to ground-based TCCON data and model calculations, Geophys. Res. Lett., 38, L15807, doi:10.1029/2011GL047871, 2011. 10966

Patra, P. K., Takigawa, M., Ishijima, K., Choi, B.-C., Cunnold, D., Dlugokencky, E. J., Fraser, P., Gomez-Pelaez, A. J., Goo, T.-Y., Kim, J.-S., Krummel, P., Langenfelds, R., Meinhardt, F., Mukai, H., O'Doherty, S., Prinn, R. G., Simmonds, P., Steele, P., Tohjima, Y., Tsuboi, K., Uhse, K., Weiss, R., Worthy, D., and Nakazawa, T.: Growth rate, seasonal, synoptic, diurnal variations and budget of methane in the lower atmosphere, J. Meteorol. Soc. Jpn., 87, 635–663, doi:10.2151/jmsj.87.635, 2009. 10969

Patra, P. K., Houweling, S., Krol, M., Bousquet, P., and Jacob, D.: Protocol for TransCom CH_4 intercomparison, 2009, version 7, http://transcom.project.asu.edu/pdf/transcom/T4.methane.protocol_v7.pdf (last access: April 2013), 2010. 10972

ACPD
13, 10961–11021, 2013

Patra, P. K., Houweling, S., Krol, M., Bousquet, P., Belikov, D., Bergmann, D., Bian, H., Cameron-Smith, P., Chipperfield, M. P., Corbin, K., Fortems-Cheiney, A., Fraser, A., Gloor, E., Hess, P., Ito, A., Kawa, S. R., Law, R. M., Loh, Z., Maksyutov, S., Meng, L., Palmer, P. I., Prinn, R. G., Rigby, M., Saito, R., and Wilson, C.: TransCom model simulations of CH_4 and related species: linking transport, surface flux and chemical loss with CH_4 variability in the troposphere and lower stratosphere, Atmos. Chem. Phys., 11, 12813–12837, doi:10.5194/acp-11-12813-2011, 2011. 10965, 10967, 10968, 10972, 10975, 10979, 10985

Peylin, P., Rayner, P. J., Bousquet, P., Carouge, C., Hourdin, F., Heinrich, P., Ciais, P., and AEROCARB contributors: Daily CO_2 flux estimates over Europe from continuous atmospheric measurements: 1, inverse methodology, Atmos. Chem. Phys., 5, 3173–3186, doi:10.5194/acp-5-3173-2005, 2005. 10973

Pickett-Heaps, C. A., Jacob, D. J., Wecht, K. J., Kort, E. A., Wofsy, S. C., Diskin, G. S., Worthy, D. E. J., Kaplan, J. O., Bey, I., and Drevet, J.: Magnitude and seasonality of wetland methane emissions from the Hudson Bay Lowlands (Canada), Atmos. Chem. Phys., 11, 3773–3779, doi:10.5194/acp-11-3773-2011, 2011. 10970

Pison, I., Bousquet, P., Chevallier, F., Szopa, S., and Hauglustaine, D.: Multi-species inversion of CH_4, CO and H_2 emissions from surface measurements, Atmos. Chem. Phys., 9, 5281–5297, doi:10.5194/acp-9-5281-2009, 2009. 10965, 10969, 10971

Prather, M.: Numerical advection by conservation of second-order moments, J. Geophys. Res., 91, 6671–6681, doi:10.1029/JD091iD06p06671, 1986. 10969, 11004

Rasch, P. and Kristjánsson, J.: A comparison of the CCM3 model climate using diagnosed and predicted condensate parameterizations, J. Climate, 11, 1587–1614, doi:10.1175/1520-0442(1998)011<1587:ACOTCM>2.0.CO;2, 1998. 10970, 11004

Rigby, M., Prinn, R. G., Fraser, P. J., Simmonds, P. G., Langenfelds, R. L., Huang, J., Cunnold, D. M., Steele, L. P., Krummel, P. B., Weiss, R. F., O'Doherty, S., Salameh, P. K., Wang, H. J., Harth, C. M., Mühle, J., and Porter, L. W.: Renewed growth of atmospheric methane, Geophys. Res. Lett., 35, L22805, doi:10.1029/2008GL036037, 2008. 10964

Rödenbeck, C., Houweling, S., Gloor, M., and Heimann, M.: CO_2 flux history 1982–2001 inferred from atmospheric data using a global inversion of atmospheric transport, Atmos. Chem. Phys., 3, 1919–1964, doi:10.5194/acp-3-1919-2003, 2003. 10973

Rotman, D. A.: IMPACT, the LLNL 3-D global atmospheric chemical transport model for the combined troposphere and stratosphere: model description and analysis of ozone and other trace gases, J. Geophys. Res., 109, D04303, doi:10.1029/2002JD003155, 2004. 10969

Russell, G. and Lerner, J.: A new finite-differencing scheme for the tracer transport equation, J. Appl. Meteorol., 20, 1483–1498, doi:10.1175/1520-0450(1981)020<1483:ANFDSF>2.0.CO;2, 1981. 10969, 11004

Saito, R., Patra P., Sweeney, C., Machida, T., Krol, M., Houweling, S., Bousquet, P., Agustipanareda, A., Belikov, D., Bergmann, D., Bian, H., Cameron-Smith, P., Chipperfield, M., Fortems-Cheney, A., Fraser, A., Gatti, M., Gloor, E., Hess, P., Kawa, S., Law, R., Locatelli, R., Loe, Z., Maksyutov, S., Meng, L., Miller, J., Palmer, P., Prinn, R., Rigby, M., and Wilson, C.: TransCom model simulations of methane: comparison of vertical profiles with in situ aircraft measurements, J. Geophys. Res., doi:10.1002/jgrd.50380, accepted, 2013. 10987, 10991

Simpson, I. J., Sulbaek Andersen, M. P., Meinardi, S., Bruhwiler, L., Blake, N. J., Helmig, D., Rowland, F. S., and Blake, D. R.: Long-term decline of global atmospheric ethane concentrations and implications for methane, Nature, 488, 490–494, doi:10.1038/nature11342, 2012. 10964

Spahni, R., Chappellaz, J., Stocker, T. F., Loulergue, L., Hausammann, G., Kawamura, K., Flückiger, J., Schwander, J., Raynaud, D., Masson-Delmotte, V., and Jouzel, J.: Atmospheric methane and nitrous oxide of the Late Pleistocene from Antarctic ice cores, Science, 310, 1317–1321, doi:10.1126/science.1120132, 2005. 10964

Spivakovsky, C. M., Logan, J. A., Montzka, S. A., Balkanski, Y. J., Foreman-Fowler, M., Jones, D. B. A., Horowitz, L. W., Fusco, A. C., Brenninkmeijer, C. A. M., Prather, M. J., Wofsy, S. C., and McElroy, M. B.: Three-dimensional climatological distribution of tropospheric OH: update and evaluation, J. Geophys. Res., 105, 8931, doi:10.1029/1999JD901006, 2000. 10971

Stephens, B. B., Gurney, K. R., Tans, P. P., Sweeney, C., Peters, W., Bruhwiler, L., Ciais, P., Ramonet, M., Bousquet, P., Nakazawa, T., Aoki, S., Machida, T., Inoue, G., Vinnichenko, N., Lloyd, J., Jordan, A., Heimann, M., Shibistova, O., Langenfelds, R. L., Steele, L. P., Francey, R. J., and Denning, A. S.: Weak northern and strong tropical land carbon uptake from vertical profiles of atmospheric CO_2, Science, 316, 1732–1735, doi:10.1126/science.1137004, 2007. 10990

Taguchi, S., Law, R. M., Rödenbeck, C., Patra, P. K., Maksyutov, S., Zahorowski, W., Sartorius, H., and Levin, I.: TransCom continuous experiment: comparison of ^{222}Rn transport at hourly time scales at three stations in Germany, Atmos. Chem. Phys., 11, 10071–10084, doi:10.5194/acp-11-10071-2011, 2011. 10965

Tarantola, A.: Inverse Problem Theory, Society for Industrial and Applied Mathematics, Philiadelphia, USA, 2005. 10971

Tiedtke, M.: A comprehensive mass flux scheme for cumulus parameterization in large-scale models, Mon. Weather Rev., 117, 1779–1800, doi:10.1175/1520-0493(1989)117<1779:ACMFSF>2.0.CO;2, 1989. 10970, 11004

van der Werf, G. R., Randerson, J. T., Giglio, L., Collatz, G. J., Mu, M., Kasibhatla, P. S., Morton, D. C., DeFries, R. S., Jin, Y., and van Leeuwen, T. T.: Global fire emissions and the contribution of deforestation, savanna, forest, agricultural, and peat fires (1997–2009), Atmos. Chem. Phys., 10, 11707–11735, doi:10.5194/acp-10-11707-2010, 2010. 10980

Walton, J., MacCracken, M., and Ghan, S.: A global-scale Lagrangian trace species model of transport, transformation, and removal processes, J. Geophys. Res., 93, 8339–8354, doi:10.1029/JD093iD07p08339, 1988. 10969, 11004

Yver, C. E., Pison, I. C., Fortems-Cheiney, A., Schmidt, M., Chevallier, F., Ramonet, M., Jordan, A., Søvde, O. A., Engel, A., Fisher, R. E., Lowry, D., Nisbet, E. G., Levin, I., Hammer, S., Necki, J., Bartyzel, J., Reimann, S., Vollmer, M. K., Steinbacher, M., Aalto, T., Maione, M., Arduini, J., O'Doherty, S., Grant, A., Sturges, W. T., Forster, G. L., Lunder, C. R., Privalov, V., Paramonova, N., Werner, A., and Bousquet, P.: A new estimation of the recent tropospheric molecular hydrogen budget using atmospheric observations and variational inversion, Atmos. Chem. Phys., 11, 3375–3392, doi:10.5194/acp-11-3375-2011, 2011. 10973

Zhang, G. and McFarlane, N.: Sensitivity of climate simulations to the parameterization of cumulus convection in the Canadian Climate Centre general circulation model, Atmos. Ocean, 33, 407–446, doi:10.1080/07055900.1995.9649539, 1995. 10970, 11004

ACPD

13, 10961–11021, 2013

Title Page
Abstract | Introduction
Conclusions | References
Tables | Figures
◀| |▶
◀ ▶
Back | Close
Full Screen / Esc
Printer-friendly Version
Interactive Discussion

Table 1. Main characteristics (vertical resolution, horizontal resolution and meteorological drivers) of the TransCom models used in this experiment.

Model Name	Vertical Resolution[1]	Horizontal resolution	Meteorological fields
ACTM	67σ	$2.8^\circ \times 2.8^\circ$	NCEP2
IFS	60η	$0.7^\circ \times 0.7^\circ$	ERA-interim
IMPACT	55η	$5.0^\circ \times 4.0^\circ$	NASA/GSFC/GEOS 4
IMPACT-1 × 1	55η	$1.25^\circ \times 1.0^\circ$	NASA/GSFC/GEOS 4
LMDZ-SACS	$\boldsymbol{19\eta}$	$\boldsymbol{3.75^\circ \times 2.5^\circ}$	**ECMWF**
MOZART	28σ	$1.8^\circ \times 1.8^\circ$	NCEP/NCAR
PCTM	58η	$1.25^\circ \times 1.0^\circ$	NASA/GSFC/GEOS 5
TM 5	25η	$6.0^\circ \times 4.0^\circ$	ECMWF, ERA-interim
TM 5-1 × 1	25η	$1.0^\circ \times 1.0^\circ$	ECMWF, ERA-interim
TOMCAT	60η	$2.8^\circ \times 2.8^\circ$	ECMWF, ERA-40/interim

[1] σ vertical coordinates are pressure divided by surface pressure, η vertical coordinates are a hybrid sigma-pressure coordinate.

ACPD
13, 10961–11021, 2013

ACPD
13, 10961–11021, 2013

Transport model errors in methane inversions

R. Locatelli et al.

Table 2. Main transport and subgrid parameterisation schemes (advection, convection and planetary boundary layer (PBL) schemes) of the TransCom models used in this experiment.

Model Name	Advection scheme	Convection scheme	PBL mixing scheme
ACTM	(Lin and Rood, 1996)	(Arakawa and Schubert, 1974)	(Holtslag, 1993)
IFS	(Hortal, 2002)	(Bechtold et al., 2008)	(Köhler et al., 2011)
IMPACT	(Lin and Rood, 1996)	(Rasch and Kristjánsson, 1998)	(Walton et al., 1988)
LMDZ-SACS	**(Leer, 1977; Hourdin and Armengaud, 1999)**	**(Tiedtke, 1989)**	**(Laval et al., 1981)**
MOZART	(Lin and Rood, 1996)	(Zhang and McFarlane, 1995)	(Holtslag, 1993)
PCTM	(Lin and Rood, 1996)	similar to (Tiedtke, 1989)	(Louis, 1979) for stable, (Lock et al., 2000) for unstable
TM 5	(Russell and Lerner, 1981)	(Tiedtke, 1989)	(Louis, 1979; Holtslag and Moeng, 1991)
TOMCAT	(Prather, 1986)	(Tiedtke, 1989)	(Holtslag, 1993)

Table 3. Estimates of hemispheric methane fluxes in teragram of methane per year ($TgCH_4\,yr^{-1}$) for every TransCom model inversion. Inverted fluxes in the Northern (NH) and in the Southern Hemisphere (SH) are presented in the first two columns. The inter-hemispheric gradient (NH estimate – SH estimate) is shown in the third column.

	Northern Hemisphere	Southern Hemisphere	Difference NH–SH
Target Flux	**368**	**155**	**213**
ACTM	391	142	249
IFS	388	150	238
IMPACT	385	148	237
IMPACT-1 × 1	385	152	233
MOZART	378	145	233
PCTM	410	140	270
TM 5	429	116	313
TM5-1 × 1	414	133	281
TOMCAT	387	144	243

ACPD
13, 10961–11021, 2013

Table 4. Errors (in ppb) contained in **R** matrix of Chen and Prinn (2006), Bergamaschi et al. (2005) and our study at 25 surface stations.

ID	station name	(Chen and Prinn, 2006)	(Bergamaschi et al., 2005)	Our study
ALT	Alert, Nunavut, Canada	6.5	5.4	6.0
ZEP	Ny-Alesund, Svalbard, Spitsbergen	13.3	6.8	9.3
BRW	Barrow, Alaska, USA	21.9	12.2	13.7
BAL	Baltic Sea, Poland	30.1	14.8	27.0
CBA	Cold Bay, Alaska, USA	8.7	10.8	10.7
MHD	Mace Head, Ireland	15.4	21.0	11.9
HUN	Hegyatsal, Hungary	101.2	26.5	41.0
LEF	Park Falls, Wisconsin, USA	21.9	13.0	22.8
BSC	Black Sea, Constanta, Romania	46.4	41.9	43.1
KZM	Plateau Assy, Kazakhstan	22.4	15.3	19.3
NWR	Niwot Ridge, Colorado, USA	16.3	8.3	19.2
UTA	Wendover, Utah, USA	27.7	13.2	20.7
TAP	Tae-ahn Peninsula, Republic of Korea	54.9	33.1	40.3
WLG	Mt. Waliguan, Peoples Republic of China	22.5	17.5	15.2
BME	St. Davis Head, Bermuda	17.5	11.5	18.9
WIS	Sede Boker, Negev Desert, Israel	17.8	13.6	23.9
ASK	Assekrem, Algeria	11.2	5.7	7.7
MLO	Mauna Loa, Hawai, USA	6.5	9.3	10.8
KUM	Cape Kumukahi, Hawai, USA	10.6	8.5	10.0
RPB	Ragged Point, Barbados	5.5	8.9	10.7
ASC	Ascension Island	5.8	6.4	5.1
SMO	Cape Matatula, Tutuila, American Samoa	4.9	7.6	7.9
CGO	Cape Grim, Tasmania, Australia	5.2	8.9	5.8
SPO	South Pole, Antarctica	7.6	3.0	1.6
	Average over all stations	**20.9**	**13.5**	**15.9**

Discussion Paper | Discussion Paper | Discussion Paper | Discussion Paper |
ACPD
13, 10961–11021, 2013
Transport model errors in methane inversions
R. Locatelli et al.

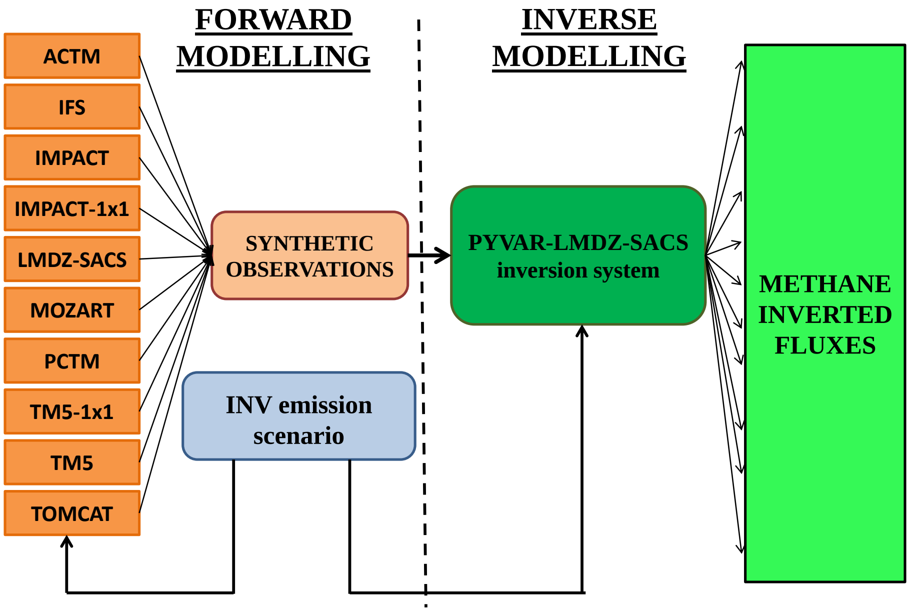

Fig. 1. Scheme of the methodology of our experiment. Synthetic observations are created from the outputs of TransCom-CH_4 forward modelling simulations. INV scenario is used both as CH_4 fluxes for forward modelling and as prior fluxes for inversions. Several CH_4 fluxes are derived using PYVAR-LMDZ-SACS inversion system for 2005.

ACPD
13, 10961–11021, 2013

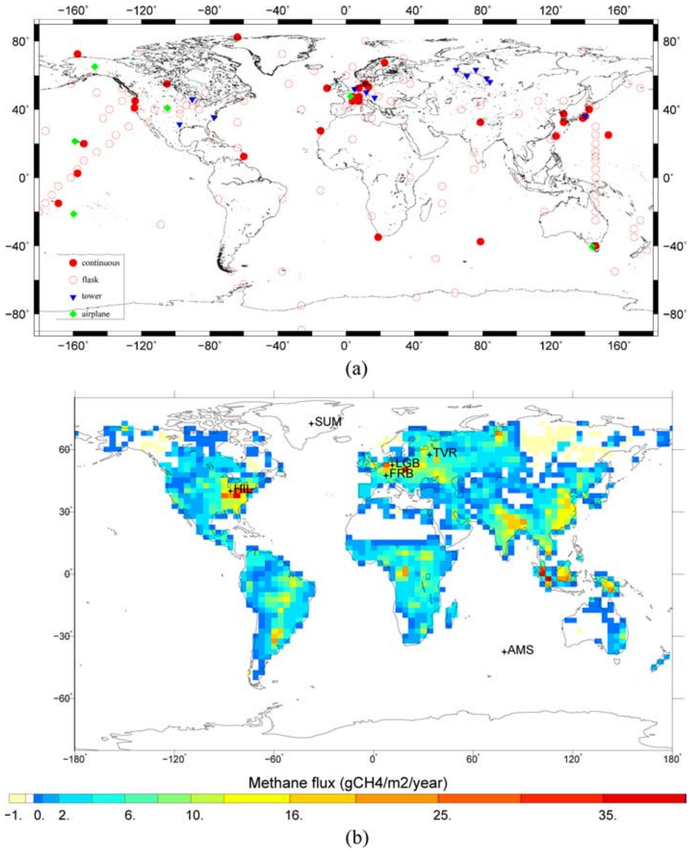

Fig. 2. Geographical representation of the two main inversion components: atmospheric constraint locations and INV emission scenario. **(a)** Map of the synthetic measurement locations. **(b)** INV emission scenario in $g\,CH_4\,m^{-2}\,yr^{-1}$.

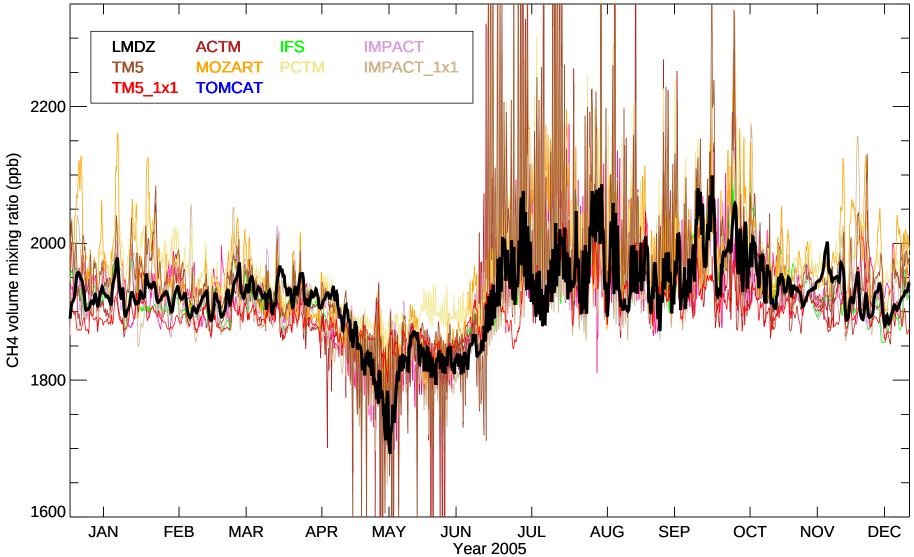

Fig. 3. Time series of daily CH_4 mixing ratio at Karasevoe (58.25° N, 82.40° E) for 2005. Each TransCom model is represented by a specific color, while LMDZ-SACS is represented by the black line.

ACPD
13, 10961–11021, 2013

Transport model errors in methane inversions

R. Locatelli et al.

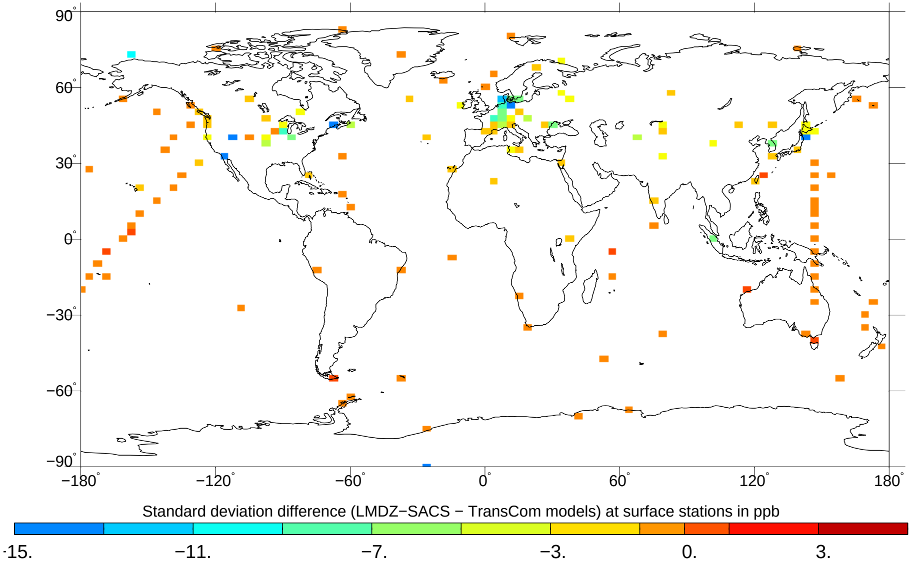

Fig. 4. Map of the difference of the "synoptic" standard deviation (STD) computed for CH_4 mixing ratio simulated by LMDZ-SACS and TransCom models at surface stations ($\sigma_{\text{LMDZ-SACS}} - \overline{\sigma_{\text{TransCom}}}$; $\overline{\sigma_{\text{TransCom}}}$ is the average of all TransCom models STD). The synoptic STD difference is expressed in ppb.

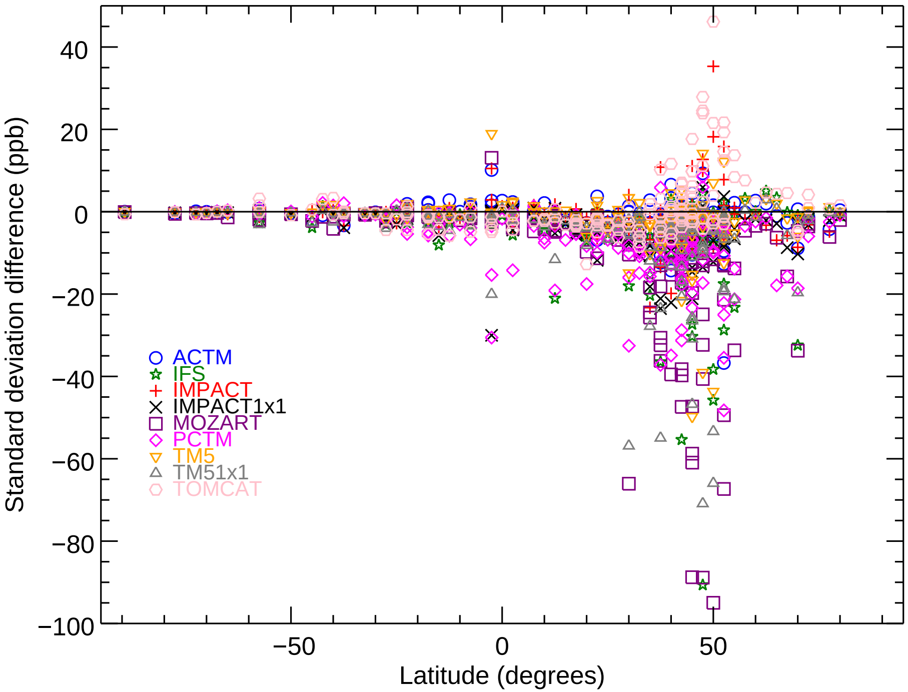

Fig. 5. Latitudinal distribution of the "synoptic" standard deviation (STD) difference between LMDZ-SACS and other TransCom models at all surface stations ($\sigma_{\text{LMDZ-SACS}} - \sigma_{(\text{TransCom model})_i}$). Each TransCom model is represented by a specific symbol. The STD difference is expressed in ppb.

ACPD
13, 10961–11021, 2013

Transport model errors in methane inversions

R. Locatelli et al.

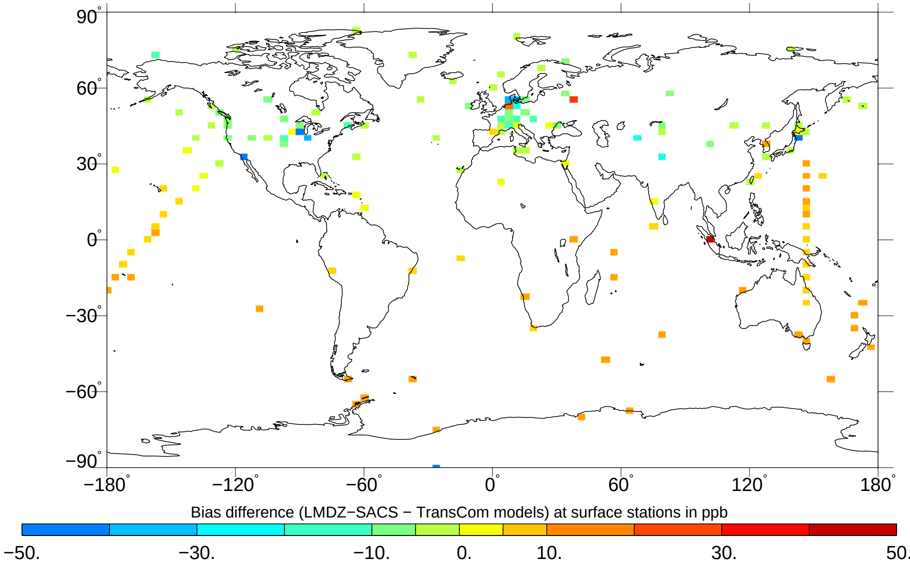

Fig. 6. Bias between CH_4 mixing ratio simulated by LMDZ-SACS and TransCom models ($y_{LMDZ} - \overline{y_{TransCom}}$; $\overline{y_{TransCom}}$ is the average of CH_4 mixing ratios simulated by all TransCom models) at surface stations. The bias is expressed in ppb.

ACPD
13, 10961–11021, 2013

Transport model errors in methane inversions

R. Locatelli et al.

ACPD
13, 10961–11021, 2013

Transport model errors in methane inversions

R. Locatelli et al.

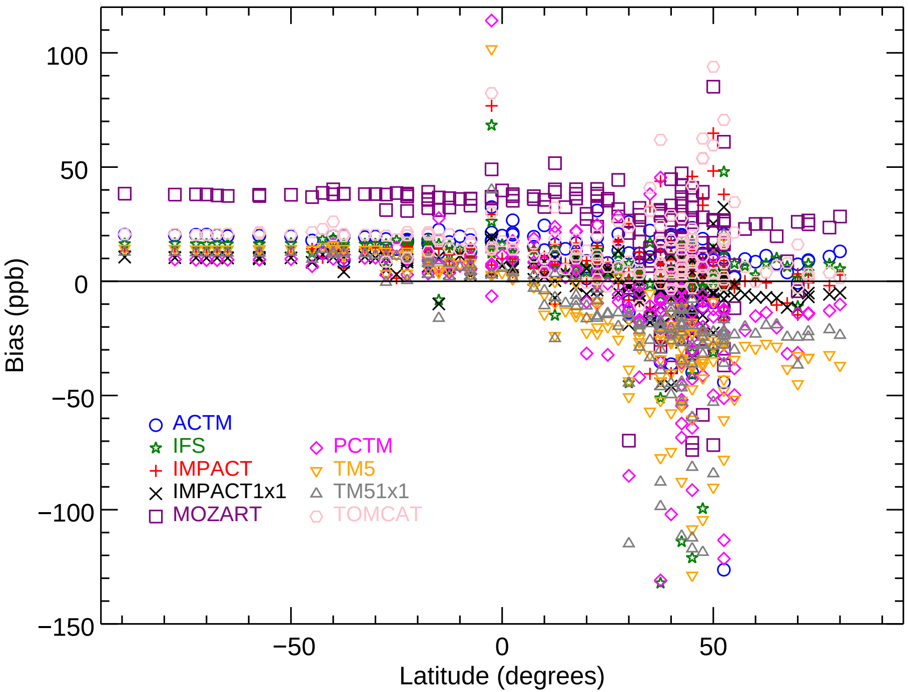

Fig. 7. Latitudinal distribution of the bias between CH_4 mixing ratio simulated by LMDZ-SACS and TransCom models ($y_{LMDZ} - y_{(TransCom\ model)_i}$) at all surface stations. Each TransCom model is represented by a specific symbol. The bias is expressed in ppb.

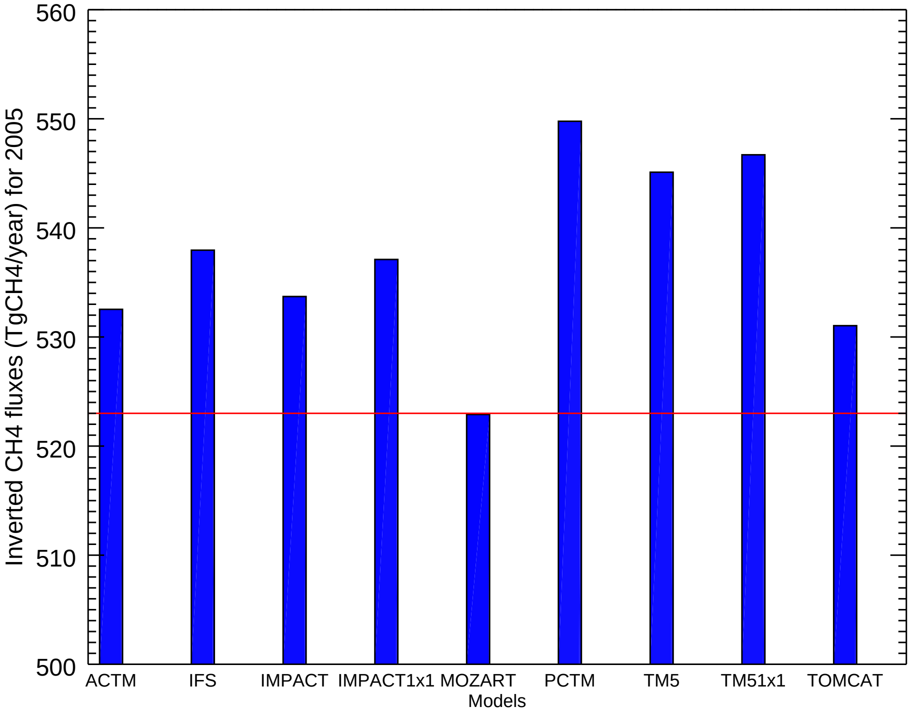

Fig. 8. Inverted CH_4 fluxes for every TransCom model at the global scale in 2005. The red line represents the value of the target methane flux at the global scale (523 Tg CH_4 in 2005, INV scenario).

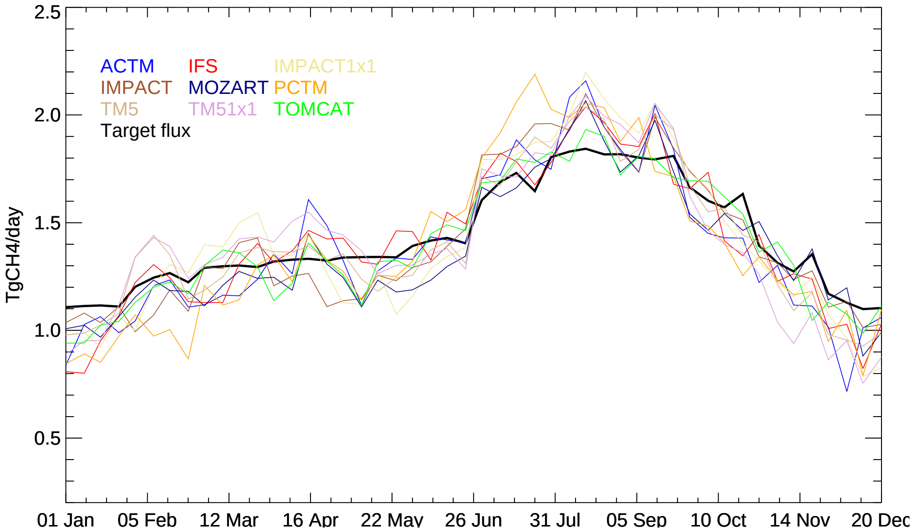

Fig. 9. Time series of weekly estimated CH_4 fluxes at the global scale for every TransCom model. The black line represents the time series of the target flux.

ACPD
13, 10961–11021, 2013

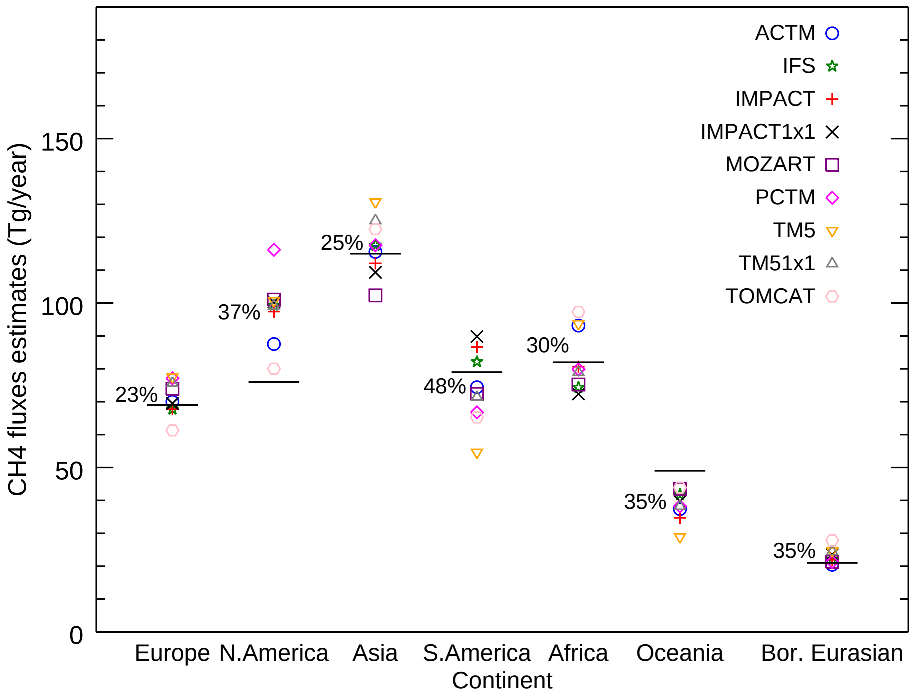

Fig. 10. Inverted CH_4 fluxes at regional scale. Seven continental regions are exposed here (Europe, north America, Asia, south America, Africa, Oceania and Boreal Eurasian). Every symbol shows the estimate value for a specific TransCom model and for a specific region. The percentage indicates the spread of the whole estimates for every region. The black lines exhibit the target methane regional estimates.

ACPD
13, 10961–11021, 2013

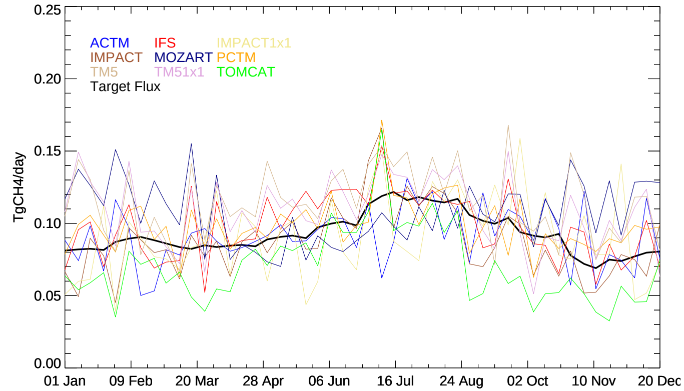

(a)

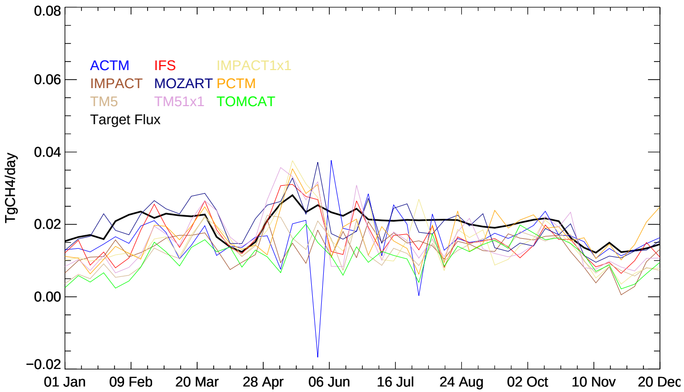

(b)

Fig. 11. Time series of weekly estimated CH_4 fluxes in $TgCH_4$ per day for **(a)** Western Europe and **(b)** Oceania. The black line represents the time series of the target flux.

ACPD
13, 10961–11021, 2013

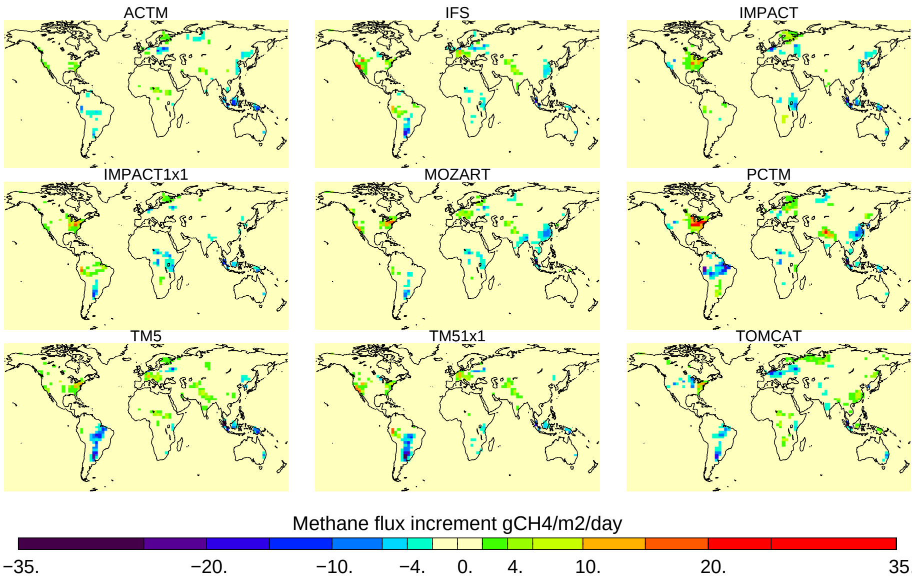

Fig. 12. Panel showing the differences between CH_4 analysed fluxes and target fluxes ($X^{\text{analysed}}_{\text{TransCom}} - X_{\text{target}}$) at gridbox scale for every TransCom model. The flux differences are expressed in $g CH_4\ m^{-2}\ day^{-1}$.

ACPD
13, 10961–11021, 2013

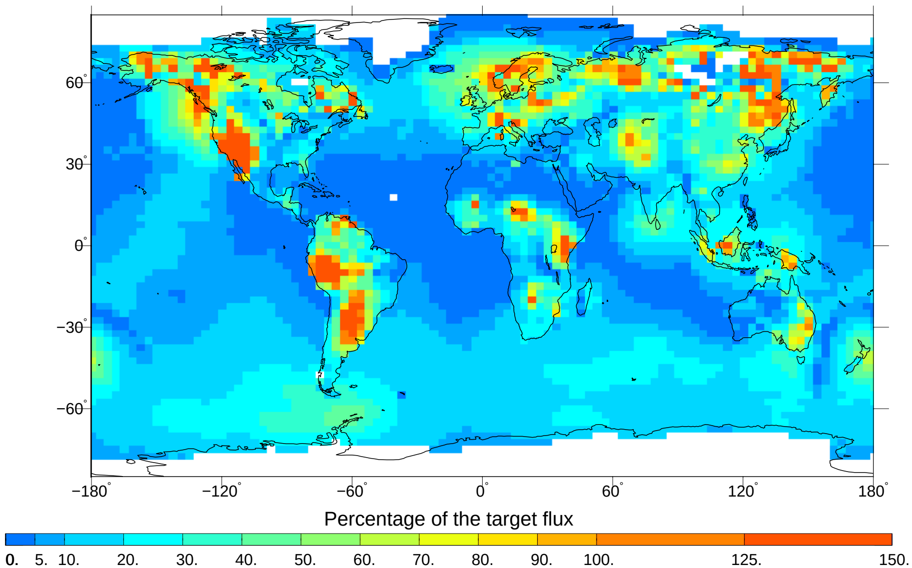

Fig. 13. Map of the spread of methane inverse estimates at model gridbox scale in percentage (%) of the target flux (INV emission scenario).

ACPD
13, 10961–11021, 2013

Transport model errors in methane inversions

R. Locatelli et al.

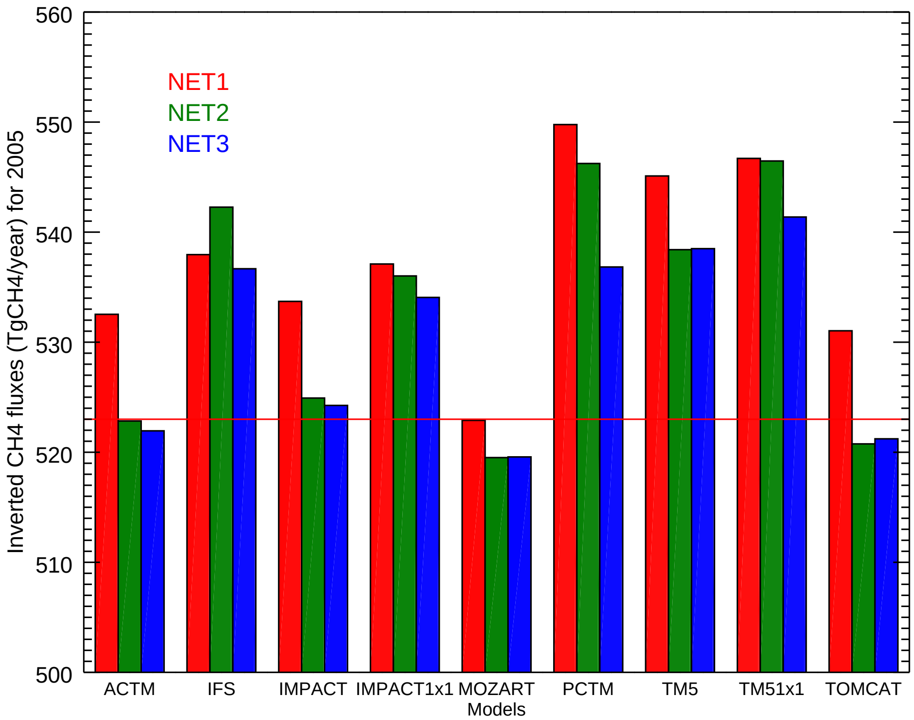

Fig. 14. Global methane estimates for every inversion using TransCom model outputs as synthetic observations in three network configurations. Results for NET1, NET2 and NET3 are respectively represented in red, green and blue. The red line exposes the target value of the methane flux at the global scale (523 Tg CH_4 yr^{-1}).

ACPD
13, 10961–11021, 2013

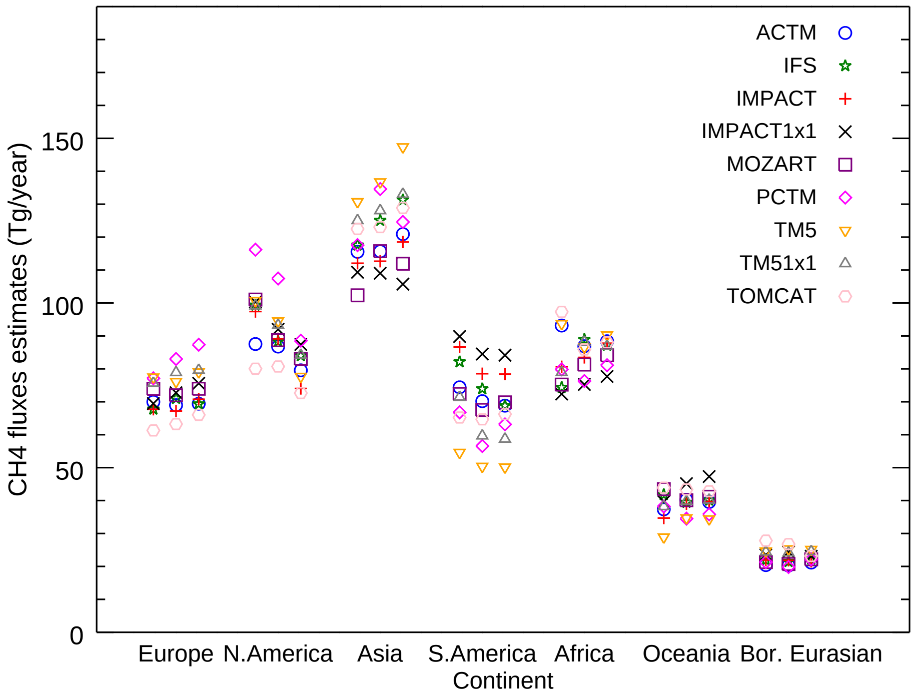

Fig. 15. Regional methane estimates for every inversion using TransCom model outputs as synthetic observations in three network configurations. Estimates for seven continental regions (Europe, north America, Asia, south America, Africa, Oceania and Boreal Eurasian) are exposed. For every continental region, the first (second and third) column represents the estimates in the NET1 (NET2 and NET3, respectively) configuration.

ACPD
13, 10961–11021, 2013